

Revista Mexicana de Astronomía y Astrofísica

Revista Mexicana de Astronomía y Astrofísica
Universidad Nacional Autónoma de México
rmaa@astroscu.unam.mx
ISSN (Versión impresa): 0185-1101
MÉXICO

2007

J. García Rojas / C. Esteban / A. Peimbert / M. Rodríguez / M. Peimbert / M. T. Ruiz
THE CHEMICAL COMPOSITION OF THE GALACTIC H II REGIONS M8 AND M17. A
REVISION BASED ON DEEP VLT ECHELLE SPECTROPHOTOMETRY
Revista Mexicana de Astronomía y Astrofísica, año/vol. 43, número 001
Universidad Nacional Autónoma de México
Distrito Federal, México
pp. 3-31

Red de Revistas Científicas de América Latina y el Caribe, España y Portugal

Universidad Autónoma del Estado de México

<http://redalyc.uaemex.mx>



THE CHEMICAL COMPOSITION OF THE GALACTIC H II REGIONS M8 AND M17. A REVISION BASED ON DEEP VLT ECHELLE SPECTROPHOTOMETRY⁵

J. García-Rojas,¹ C. Esteban,¹ A. Peimbert,² M. Rodríguez,³ M. Peimbert,² and M. T. Ruiz⁴

Received 2006 July 7; accepted 2006 October 2

RESUMEN

Presentamos nuevos datos espectrofotométricos de las regiones H II Galácticas M8 y M17. Los datos se obtuvieron a través del espectrógrafo echelle UVES del VLT en el intervalo entre los 3100 y los 10400 Å. Medimos las intensidades de 375 y 260 líneas de emisión en M8 y M17, respectivamente, incrementando de forma significativa el número de líneas identificadas en estas nebulosas. La mayoría de las líneas detectadas son permitidas. Calculamos las temperaturas y densidades electrónicas usando diferentes diagnósticos, y determinamos las abundancias iónicas de He⁺, C⁺⁺, O⁺ and O⁺⁺ a partir de líneas debidas únicamente a recombinación, así como las abundancias de un gran número de iones de diferentes elementos usando líneas de excitación colisional. Obtuvimos estimaciones consistentes de t^2 usando diferentes indicadores independientes. Detectamos líneas de emisión de la serie de Balmer de deuterio en M8, hasta D ϵ ; también mostramos que sus intensidades son consistentes con el hecho de que la fluorescencia del continuo es el principal mecanismo de excitación de estas líneas.

ABSTRACT

We present new echelle spectrophotometry of the Galactic H II regions M8 and M17. The data have been taken with the VLT UVES echelle spectrograph in the 3100 to 10400 Å range. We have measured the intensities of 375 and 260 emission lines in M8 and M17 respectively, increasing significantly the number of emission lines measured in previous spectrophotometric studies of these nebulae. Most of the detected lines are permitted lines. Electron temperatures and densities have been determined using different diagnostics. We have derived He⁺, C⁺⁺, O⁺ and O⁺⁺ ionic abundances from pure recombination lines. We have also derived abundances from collisionally excited lines for a large number of ions of different elements. Highly consistent estimations of t^2 have been obtained by using different independent indicators; the values are moderate and very similar to those obtained in other Galactic H II regions. We report the detection of deuterium Balmer emission lines, up to D ϵ , in M8 and show that their intensities are consistent with continuum fluorescence as their main excitation mechanism.

Key Words: H II REGIONS — ISM: ABUNDANCES — ISM: INDIVIDUAL: M8, M17 — LINE: IDENTIFICATION

¹Instituto de Astrofísica de Canarias, Spain.

²Instituto de Astronomía, Universidad Nacional Autónoma de México, Mexico.

³Instituto Nacional de Astrofísica, Óptica y Electrónica, Mexico.

⁴Departamento de Astronomía, Universidad de Chile, Chile.

⁵Based on observations collected at the European Southern Observatory, Chile, proposal number ESO 68.C-0149(A).

1. INTRODUCTION

This is the last of a series of 5 papers devoted to present results of long-exposure high-spectral-resolution spectral data taken with the VLT UVES echelle spectrograph with the aim of obtaining accurate measurements of very faint permitted lines of heavy element ions in Galactic H II regions. Our

sample consists of eight of the brightest Galactic H II regions which cover a range of Galactocentric distances from 6.3 to 10.4 kpc (assuming the Sun to be at 8 kpc from the Galactic center). The objects whose data have already been published are: NGC 3576 (García-Rojas et al. 2004), the Orion Nebula (Esteban et al. 2004), S 311 (García-Rojas et al. 2005), M16, M20, and NGC 3603 (García-Rojas et al. 2006).

Along this project we have detected and measured an unprecedented large number of emission lines in all the H II regions analyzed, which could improve the knowledge of the nebular gas conditions and abundances. We have derived chemical abundances of C^{++} and O^{++} from several recombination lines of C II and O II, avoiding the problem of line blending in all the H II regions of our sample. The high signal-to-noise ratio of the VLT spectra of M8 and M17 has allowed us to detect and measure more C^{++} and O^{++} RLs than in previous works (i.e., Esteban et al. 1999b, hereinafter EPTGR, in M8 and Esteban et al. 1999a, hereinafter EPTG, in M17); also, the reliability of the line determinations has increased significantly with respect to the previous detections. From the observations of all the objects of our project, Esteban et al. (2005) obtained –for the first time– the radial gas-phase C and O gradients of the Galactic disk making use of RLs, which are, in principle, better for abundance determinations because the ratio X^{+p}/H^{+} from RLs is almost-independent of the temperature structure of the nebula. A reliable determination of these gradients is of paramount importance for chemical evolution models of our Galaxy (see Carigi et al. 2005).

The fact that ionic abundances determined from the intensity of collisionally excited lines (CELs) are systematically lower (with factors ranging from 1.3 to 2.8) than those determined by recombination lines (RLs) is far from being completely understood, and has led to the so-called “abundance discrepancy” problem. This problem is clearly present in Galactic H II regions (see Peimbert, Torres-Peimbert, & Dufour 1993; Tsamis et al. 2003, and all papers related to this project). In the case of extragalactic studies, only a few works have been developed with the aim of detecting the faint recombination lines: Esteban et al. (2002) for M33 and M101, Peimbert (2003) and Tsamis et al. (2003) for the Magellanic Clouds, Peimbert, Peimbert, & Ruiz (2005) for NGC 6822. Moreover, López-Sánchez et al. (2007) have, for NGC 5253, estimated abundance discrepancies rather similar to those of the Galactic objects.

One of the probable causes of the abundance discrepancy is the presence of spatial variations in the temperature structure of the nebulae (Torres-Peimbert, Peimbert, & Daltabuit 1980). Temperature fluctuations may produce the discrepancy due to the different functional dependence of the line emissivities of CELs and RLs on the electron temperature, which is stronger –exponential– in the case of CELs. Temperature fluctuations have been parametrized traditionally by t^2 , the mean-square temperature fluctuation of the gas (see Peimbert 1967; Peimbert & Costero 1969; Peimbert 1971, for a detailed formulation). It is a well known result that photoionization codes cannot reproduce the temperature fluctuations found in gaseous nebulae, but there are mainly two possibilities to explain them: first, there might be an additional important source of energy producing such fluctuations, which has not been taken into account by photoionization models; second, there could be density inhomogeneities (Viegas & Clegg 1994) or chemical inhomogeneities (see Tsamis & Péquignot 2005, and references therein) that produce temperature variations. The physical processes that may cause such temperature fluctuations are still a subject of controversy. Reviews of the relevant processes can be found in Esteban (2002), Torres-Peimbert & Peimbert (2003), and Peimbert & Peimbert (2006). Additionally, there are some very recent works devoted to this topic: e.g., Giammanco & Beckman (2005) have proposed ionization by cosmic rays as an additional source of energy to reproduce the temperature fluctuations observed in H II regions; and Tsamis & Péquignot (2005) have developed photoionization models for 30 Doradus in the Large Magellanic Cloud that reproduce observed temperature fluctuations through chemical inhomogeneities (inclusions) due to the infall of material nucleosynthetically processed in supernova events. Further studies are needed to understand this problem.

Several spectrophotometric works devoted to the chemical composition of M8 and M17 have been carried out previously. For M8, there are several low and intermediate spectral resolution studies (Rubin 1969; Peimbert & Costero 1969; Sánchez & Peimbert 1991; Peimbert et al. 1993; Rodríguez 1999b) and one high spectral resolution study (EPTGR). The chemical abundances of M17 have been studied using low resolution spectroscopy (Rubin 1969; Peimbert & Costero 1969; Peimbert, Torres-Peimbert, & Ruiz 1992; Rodríguez 1999b; Tsamis et al. 2003) and high-spectral resolution data (EPTG).

In this paper we make a reappraisal of the chemical composition of M8 and M17 in the same slit po-

sition observed by EPTGR in M8 and in one of the positions observed by EPTG in M17 (position 14), by means of new echelle spectrophotometry obtained with the ESO Very Large Telescope. Our new observations increase significantly the number of lines detected and the quality of the measured line intensities for these two nebulae.

In §§ 2 and 3 we describe the observations, the data reduction, and line intensity determination procedures. In § 4 we obtain temperatures and densities using several diagnostic ratios. In § 5 we briefly analyze the recombination spectra of He I and derive the He^+/H^+ ratio. In § 6 we give the ionic abundances determined from CELs. In § 7 we use RLs to derive O and C ionic abundances. In § 8 we present the total abundances. We report the detection of deuterium Balmer lines in § 9. In §§ 10 and 11 we present the comparison with previous results and the conclusions, respectively.

2. OBSERVATIONS AND DATA REDUCTION

The observations were made on 2002 March 11 with the Ultraviolet Visual Echelle Spectrograph, UVES (D’Odorico et al. 2000), at the VLT Kueyen Telescope in Cerro Paranal Observatory (Chile). We used the standard settings in both the red and blue arms of the spectrograph, covering the region from 3100 to 10400 Å. The log of the observations is presented in Table 1.

TABLE 1
JOURNAL OF OBSERVATIONS

$\Delta\lambda$ (Å)	Exp. time (s)	
	M8	M17
3000–3900	30, 3 × 300	30, 3 × 300
3800–5000	30, 3 × 800	60, 3 × 800
4700–6400	30, 3 × 300	30, 3 × 300
6300–10400	30, 3 × 800	60, 3 × 800

The wavelength regions 5783–5830 Å and 8540–8650 Å were not observed due to a gap between the two CCDs used in the red arm. There are also five small gaps that were not observed, 9608–9612 Å, 9761–9767 Å, 9918–9927 Å, 10080–10093 Å and 10249–10264 Å, because the five redmost orders did not fit completely within the CCD. We took long and short exposure spectra to check for possible saturation effects.

The slit was oriented east-west and the atmospheric dispersion corrector (ADC) was used to keep

the same observed region within the slit regardless of the air mass value (the averaged $\sec z$ are ~ 1.4 for M17 and ~ 1.85 for M8). The slit width was set to 3.0'' and the slit length was set to 10'' in the blue arm and to 12'' in the red arm; the slit width was chosen to maximize the S/N ratio of the emission lines and to maintain the required resolution to separate most of the weak lines needed for this project. The effective resolution for the lines at a given wavelength is approximately $\Delta\lambda \sim \lambda/8800$. The center of the slit was located in the same position as in EPTGR for M8 (labeled as HGS) and is coincident with position 14 of EPTG for M17. The final 1D spectra were extracted from an area of 3'' × 8.3''.

The spectra were reduced using the IRAF⁶ echelle reduction package, following the standard procedure of bias subtraction, flatfielding, aperture extraction, wavelength calibration and flux calibration. The standard star EG 247 was observed for flux calibration. We have not attempted sky subtraction from the spectra due to the slit length being much smaller than the objects; also, the spectral resolution of our data permit us to clearly distinguish among the telluric lines and the nebular ones.

3. LINE INTENSITIES AND REDDENING CORRECTION

Line intensities were measured integrating all the flux in the line between two given limits and over a local continuum estimated by eye. In the cases of line blending, a multiple Gaussian profile fit procedure was applied to obtain the line flux of each individual line. Most of these measurements were made with the SPLIT routine of the IRAF package. In some cases of very tight blends or blends with very bright telluric lines the analysis was performed via Gaussian fitting making use of the Starlink DIPSO software (Howarth & Murray 1990).

Table 2 presents the emission line intensities of M8 and M17, respectively. The first and fourth columns include the adopted laboratory wavelength, λ_0 , and the observed wavelength in the heliocentric framework, λ . The second and third columns show the ion and the multiplet number, or series, for each line. The fifth and sixth columns list the observed flux relative to $\text{H}\beta$, $F(\lambda)$, and the flux corrected for reddening relative to $\text{H}\beta$, $I(\lambda)$. The seventh column includes the fractional error (1σ) in the line intensities relative to $\text{H}\beta$, $I(\lambda)$. Errors were derived follow-

⁶IRAF is distributed by NOAO, which is operated by AURA, under cooperative agreement with NSF.

TABLE 2
OBSERVED AND REDDENING-CORRECTED LINE FLUXES WITH RESPECT TO $F(H\beta)=100$

λ_0 (Å)	Ion	Mult.	λ_{obs} (Å)	$F(\lambda)$	$I(\lambda)^a$	err (%) ^b	Notes
M 8							
3187.84	He I	3	3187.70	0.944	0.315	13	
3354.55	He I	8	3354.54	0.146	0.137	19	
3447.59	He I	7	3447.53	0.181	0.222	17	
3487.73	He I	42	3487.70	0.057	0.075	:	
3498.66	He I	40	3498.61	0.035	0.047	:	
3512.52	He I	38	3512.48	0.096	0.128	27	
3530.50	He I	36	3530.46	0.092	0.124	28	
3554.42	He I	34	3554.39	0.163	0.221	17	
3587.28	He I	32	3587.24	0.181	0.242	17	
3613.64	He I	6	3613.61	0.291	0.381	12	
3634.25	He I	28	3634.20	0.300	0.385	12	
3656.10	H I	H37	3656.08	0.036	0.045	:	
3657.27	H I	H36	3657.24	0.088	0.110	29	
3657.92	H I	H35	3657.89	0.106	0.134	25	
3658.64	H I	H34	3658.60	0.111	0.139	24	
3659.42	H I	H33	3659.39	0.143	0.179	19	
3660.28	H I	H32	3660.24	0.161	0.202	17	
3661.22	H I	H31	3661.18	0.196	0.246	16	
3662.26	H I	H30	3662.23	0.212	0.266	15	
3663.40	H I	H29	3663.37	0.236	0.295	14	
3664.68	H I	H28	3664.62	0.271	0.338	12	
3666.10	H I	H27	3666.05	0.299	0.374	12	
3667.68	H I	H26	3667.64	0.360	0.449	11	
3669.47	H I	H25	3669.42	0.386	0.481	10	
3671.48	H I	H24	3671.43	0.425	0.528	10	
3673.76	H I	H23	3673.71	0.461	0.573	10	
3676.37	H I	H22	3676.32	0.505	0.627	9	
3679.36	H I	H21	3679.30	0.567	0.702	9	
3682.81	H I	H20	3682.76	0.587	0.727	9	
3686.83	H I	H19	3686.79	0.652	0.805	9	
3691.56	H I	H18	3691.51	0.776	0.956	9	
3697.15	H I	H17	3697.10	0.954	1.174	8	
3703.86	H I	H16	3703.80	1.065	1.308	8	
3705.04	He I	25	3704.97	0.412	0.506	11	
3711.97	H I	H15	3711.92	1.276	1.566	8	
3721.83	[S III]	2F	3721.81	2.260	2.772	8	
3721.94	H I	H14					
3726.03	[O II]	1F	3726.01	100.407	123.200	8	
3728.82	[O II]	1F	3728.77	70.305	86.287	8	
3734.37	H I	H13	3734.32	1.908	2.343	8	
3750.15	H I	H12	3750.10	2.378	2.933	8	
3770.63	H I	H11	3770.58	3.066	3.818	8	
3784.89	He I	64	3784.88	0.019	0.023	23	
3797.90	H I	H10	3797.85	4.040	5.132	8	
3805.78	He I	63	3805.64	0.030	0.039	17	
3819.61	He I	20	3819.58	0.694	0.902	8	
	?		3831.14	0.013	0.017	30	c
3831.66	S II		3831.64	0.021	0.027	21	c
3833.57	He I	62	3833.50	0.025	0.033	18	
3835.39	H I	H9	3835.33	5.567	7.245	8	
3838.37	N II	30	3838.23	0.019	0.025	22	
3853.66	Si II	1	3853.61	0.011	0.015	33	
3856.02	Si II	1	3855.98	0.145	0.189	9	
3856.13	O II	12					
3862.59	Si II	1	3862.56	0.089	0.116	11	
3867.48	He I	20	3867.45	0.053	0.069	8	
3868.75	[Ne III]	1F	3868.63	2.874	3.751	8	
3871.60	He I	60	3871.75	0.054	0.071	11	
3888.65	He I	2	3888.93	10.850	14.177	7	

TABLE 2 (CONTINUED)

λ_0 (Å)	Ion	Mult.	λ_{obs} (Å)	$F(\lambda)$	$I(\lambda)^a$	err (%) ^b	Notes
3889.05	H I	H8					
3918.98	C II	4	3918.90	0.044	0.057	13	
3920.68	C II	4	3920.61	0.093	0.122	9	
3926.53	He I	58	3926.50	0.076	0.100	10	
3935.94	He I	57	3935.88	0.016	0.021	25	
3964.73	He I	5	3964.69	0.603	0.787	8	
3967.46	[Ne III]	1F	3967.33	0.875	1.142	8	
3969.00	D I	D7	3968.86	0.011	0.014	35	
3970.07	H I	H7	3970.02	12.141	15.842	8	
3998.76	S II	59	3998.68	0.012	0.016	32	
4008.36	[Fe III]	4F	4008.30	0.017	0.022	25	
4009.22	He I	55	4009.22	0.116	0.151	9	
4023.98	He I	54	4023.99	0.008	0.010	:	
4026.08	N II	40	4026.17	1.272	1.664	8	
4026.21	He I	18					
4068.60	[S II]	1F	4068.54	1.235	1.618	8	
4069.62	O II	10	4069.65	0.049	0.064	12	
4069.89	O II	10					
4072.15	O II	10	4072.07	0.023	0.031	19	
4076.35	[S II]	1F	4076.28	0.431	0.565	8	
4100.62	D I	D6	4100.49	0.013	0.017	30	
4101.74	H I	H6	4101.69	19.551	26.190	3	
4119.22	O II	20	4119.20	0.006	0.008	:	
4120.84	He I	16	4120.78	0.101	0.134	6	
4121.48	O II	19	4121.31	0.009	0.012	39	
4132.80	O II	19	4132.73	0.010	0.014	35	
4143.76	He I	53	4143.71	0.181	0.238	4	
4153.30	O II	19	4153.17	0.021	0.028	19	
4156.54	O II	19	4156.23	0.010	0.014	35	d
4168.97	He I	52	4168.98	0.036	0.046	13	
4169.22	O II	19					
4243.97	[Fe II]	21F	4243.95	0.019	0.024	21	
4267.15	C II	6	4267.09	0.177	0.222	4	
4276.75	O II	67b	4276.73	0.017	0.022	23	
4276.83	[Fe II]	21F					
4287.40	[Fe II]	7F	4287.33	0.047	0.058	10	
4303.61	O II	66	4303.65	0.019	0.023	21	
4303.82	O II	53					
4317.14	O II	2	4316.99	0.009	0.011	38	
4319.63	O II	2	4319.55	0.006	0.008	:	
4326.40	O I		4326.27	0.015	0.019	25	
4339.29	D I	D5	4339.14	0.016	0.019	25	
4340.47	H I	H5	4340.41	37.684	45.925	3	
4345.55	O II	65c	4345.45	0.018	0.022	22	
4345.56	O II	2					
4349.43	O II	2	4349.31	0.016	0.020	24	
4352.78	[Fe II]	21F	4352.74	0.010	0.012	37	
4359.34	[Fe II]	7F	4359.27	0.034	0.041	13	
4363.21	[O III]	2F	4363.12	0.236	0.286	4	
4366.89	O II	2	4366.73	0.013	0.015	29	
4368.15	O I	5	4368.16	0.043	0.052	11	
4368.25	O I	5					
4387.93	He I	51	4387.89	0.358	0.428	3	
4413.78	[Fe II]	7F	4413.71	0.025	0.029	17	
4416.27	[Fe II]	6F	4416.23	0.028	0.033	15	
4432.35	[Fe II]	6F	4432.40	0.006	0.007	:	
4437.55	He I	50	4437.51	0.051	0.059	10	
4452.10	[Fe II]	7F	4452.02	0.018	0.021	22	
4452.37	O II	5					
4457.95	[Fe II]	6F	4457.86	0.007	0.009	:	
4463.58	S II		4463.51	0.012	0.014	30	
4471.48	He I	14	4471.45	3.014	3.482	3	
4474.90	[Fe II]	7F	4474.82	0.008	0.009	:	

TABLE 2 (CONTINUED)

λ_0 (Å)	Ion	Mult.	λ_{obs} (Å)	$F(\lambda)$	$I(\lambda)^a$	err (%) ^b	Notes
4483.43	S II	43	4483.42	0.009	0.010	:	
4487.41	O I]		4487.35	0.010	0.011	37	c
4491.07	C II		4491.19	0.010	0.011	37	
4491.23	O II	86a					
4590.97	O II	15	4590.92	0.004	0.005	:	
4607.06	[Fe III]	3F	4607.07	0.037	0.040	12	
4607.16	N II	5					
4621.39	N II	5	4621.34	0.020	0.022	20	
4628.05	[Ni II]	4F	4628.04	0.006	0.006	:	
4630.54	N II	5	4630.48	0.026	0.028	16	
4638.86	O II	1	4638.71	0.031	0.034	14	
4641.81	O II	1	4641.69	0.040	0.043	12	
4643.06	N II	5	4643.05	0.017	0.018	23	
4649.13	O II	1	4649.02	0.039	0.041	12	
4650.84	O II	1	4650.71	0.029	0.032	15	
4658.10	[Fe III]	3F	4658.10	0.495	0.530	3	
4661.63	O II	1	4661.44	0.033	0.036	13	
4667.01	[Fe III]	3F	4666.92	0.023	0.025	18	
4676.24	O II	1	4676.16	0.016	0.017	25	
4701.62	[Fe III]	3F	4701.56	0.136	0.143	5	
4711.37	[Ar IV]	1F	4711.16	0.014	0.014	28	
4713.14	He I	12	4713.12	0.323	0.339	3	
4733.91	[Fe III]	3F	4733.88	0.045	0.046	11	
4740.16	[Ar IV]	1F	4740.00	0.012	0.013	30	
4754.83	[Fe III]	3F	4754.72	0.095	0.098	6	
4769.60	[Fe III]	3F	4769.44	0.047	0.049	10	
4777.78	[Fe III]	3F	4777.69	0.022	0.023	19	
4788.13	N II	20	4788.09	0.014	0.014	27	
4803.29	N II	20	4803.27	0.011	0.011	33	
4814.55	[Fe II]	20F	4814.47	0.028	0.029	17	
4815.51	S II	9	4815.49	0.024	0.025	19	
4860.03	D I	D4	4859.85	0.037	0.036	12	
4861.33	H I	H4	4861.27	100.000	100.000	3	
4881.00	[Fe III]	2F	4881.01	0.197	0.193	4	
4889.63	[Fe III]	4F	4889.58	0.012	0.012	30	
4889.70	[Fe III]	3F					
4921.93	He I	48	4921.88	0.952	0.924	3	
4924.50	[Fe III]	2F	4924.45	0.030	0.029	16	
4924.50	O II	28					
4930.50	[Fe III]	1F	4930.62	0.010	0.010	39	
4931.32	[O III]	1F	4931.15	0.022	0.021	23	
4958.91	[O III]	1F	4958.83	34.553	33.066	3	
4985.90	[Fe III]	2F	4985.94	0.051	0.048	11	
4987.20	[Fe III]	2F	4987.33	0.045	0.042	12	
4994.37	N II	94	4994.45	0.021	0.020	23	
5001.47	N II	19	5001.39	0.034	0.032	16	
5006.84	[O III]	1F	5006.85	101.963	95.932	3	
5011.30	[Fe III]	1F	5011.36	0.060	0.057	10	
5015.68	He I	4	5015.71	1.946	1.825	3	
5041.03	Si II	5	5041.07	0.141	0.131	5	
5047.74	He I	47	5047.80	0.204	0.189	4	
5055.98	Si II	5	5056.05	0.218	0.201	4	
5056.31	Si II	5					
5146.70	[Fe III]		5146.62	0.018	0.016	27	
5158.78	[Fe II]	19F	5158.84	0.057	0.051	10	
5191.82	[Ar III]	1F	5191.77	0.034	0.030	15	
5197.90	[N I]	1F	5197.91	0.228	0.201	4	
5200.26	[N I]	1F	5200.27	0.143	0.126	5	
5261.61	[Fe II]	19F	5261.63	0.033	0.028	16	
5270.30	[Fe III]	1F	5270.57	0.310	0.267	4	
5273.35	[Fe II]	18F	5273.40	0.019	0.016	25	
5299.00	O I	26	5298.97	0.028	0.024	18	
5342.38	C II	17.06	5342.40	0.013	0.011	35	

TABLE 2 (CONTINUED)

λ_0 (Å)	Ion	Mult.	λ_{obs} (Å)	$F(\lambda)$	$I(\lambda)^a$	err (%) ^b	Notes
5412.00	[Fe III]	1F	5412.14	0.030	0.024	17	
5432.77	S II	6	5432.90	0.018	0.015	27	
5453.81	S II	6	5453.86	0.021	0.017	23	
5512.77	O I	25	5512.63	0.018	0.015	26	
5517.71	[Cl III]	1F	5517.67	0.514	0.410	3	
5537.88	[Cl III]	1F	5537.85	0.497	0.395	3	
5555.03	O I	24	5554.91	0.024	0.019	20	
5577.34	[O I]	3F	5577.33	0.033	0.026	16	
5666.64	N II	3	5666.60	0.035	0.027	15	
5676.02	N II	3	5676.01	0.019	0.015	25	
5679.56	N II	3	5679.59	0.045	0.034	13	
5686.21	N II	3	5686.34	0.012	0.009	36	
5710.76	N II	3	5710.82	0.014	0.010	32	
5754.64	[N II]	3F	5754.58	1.275	0.952	3	
5875.64	He I	11	5875.61	13.666	9.868	3	
5927.82	N II	28	5927.83	0.019	0.014	25	
5931.79	N II	28	5931.78	0.028	0.020	18	
5957.56	Si II	4	5957.55	0.071	0.050	9	
5958.58	O I	23	5958.39	0.031	0.022	17	
5978.83	Si II	4	5978.91	0.162	0.113	5	
6046.44	O I	22	6046.27	0.083	0.057	8	
6151.27	C II	16.04	6151.53	0.014	0.009	32	
6151.54	C II	16.04					
6300.30	[O I]	1F	6300.18	1.028	0.663	3	
6312.10	[S III]	3F	6312.02	2.089	1.344	3	
6347.11	Si II	2	6347.08	0.292	0.186	4	
6363.78	[O I]	1F	6363.66	0.353	0.224	4	
6371.36	Si II	2	6371.31	0.175	0.111	5	
6401.50	[Ni III]	2F	6401.29	0.013	0.008	34	
6402.25	Ne I	1	6402.22	0.031	0.019	17	
6461.95	C II	17.04	6461.87	0.040	0.025	14	
6462.13	C II	17.04					
6527.10	[N II]	1F	6527.21	0.032	0.019	16	
6533.80	[Ni III]	2F	6533.72	0.099	0.060	7	e
6548.03	[N II]	1F	6548.02	54.367	32.924	3	
6561.04	D I	D3	6560.82	0.131	0.079	6	
6562.82	H I	H3	6562.73	445.498	286.685	3	
6578.05	C II	2	6577.99	0.437	0.262	3	
6583.41	[N II]	1F	6583.38	170.515	102.331	3	
6666.80	[Ni II]	2F	6666.72	0.016	0.009	29	
6678.15	He I	46	6678.08	4.878	2.857	3	
6716.47	[S II]	2F	6716.37	15.711	9.113	3	
6730.85	[S II]	2F	6730.76	20.899	12.078	3	
6855.88	He I	1/12	6855.90	0.010	0.005	:	f
6933.91	He I	1/13	6933.68	0.015	0.008	37	g
7002.23	O I	21	7001.98	0.099	0.054	6	
7065.28	He I	10	7065.17	5.697	3.024	3	
7111.47	C I	³ D- ³ F ⁰	7111.35	0.008	0.004	:	
7113.18	C I	³ D- ³ F ⁰	7113.06	0.007	0.003	:	
7115.17	C I	³ D- ³ F ⁰	7115.10	0.007	0.004	:	
7135.78	[Ar III]	1F	7135.72	19.253	10.038	3	
7155.14	[Fe II]	14F	7155.08	0.068	0.035	9	
7160.58	He I	1/10	7160.53	0.027	0.014	21	
7231.34	C II	3	7231.22	0.146	0.074	5	
7236.19	C II	3	7236.34	0.220	0.112	4	
7281.35	He I	45	7281.27	0.920	0.462	3	
7298.05	He I	1/9	7298.00	0.040	0.020	14	
7318.39	[O II]	2F	7318.95	1.482	0.738	3	
7319.99	[O II]	2F	7320.04	6.592	3.281	3	
7329.66	[O II]	2F	7329.61	3.824	1.899	3	
7330.73	[O II]	2F	7330.69	3.604	1.789	3	
7377.83	[Ni II]	2F	7377.77	0.098	0.048	6	
7388.17	[Fe II]	14F	7388.09	0.010	0.005	:	

TABLE 2 (CONTINUED)

λ_0 (Å)	Ion	Mult.	λ_{obs} (Å)	$F(\lambda)$	$I(\lambda)^a$	err (%) ^b	Notes
7411.61	[Ni II]	2F	7411.58	0.014	0.007	:	
7423.64	N I	3	7423.48	0.023	0.011	25	
7442.30	N I	3	7442.13	0.044	0.021	13	
7452.54	[Fe II]	14F	7452.48	0.024	0.011	24	
7459.30	Ca I]		7459.14	0.007	0.003	:	c, e
7468.31	N I	3	7468.13	0.074	0.035	8	
7477.10	Si I		7477.22	0.009	0.004	:	
7499.85	He I	1/8	7499.81	0.067	0.032	9	
	?		7513.08	0.014	0.007	39	
7519.50	C II	16.08	7519.80	0.009	0.004	:	
7519.86	C II	16.08					
7751.10	[Ar III]	2F	7751.08	5.993	2.679	3	
7771.94	O I	1	7771.86	0.066	0.029	9	
7801.79	V I		7801.71	0.006	0.002	:	c
7816.13	He I	1/7	7816.08	0.115	0.051	6	
7837.85	[Co I]		7837.64	0.017	0.007	34	
7862.85	Fe II]		7862.65	0.005	0.002	:	c
7875.99	[P II]	¹ D- ¹ S	7875.67	0.010	0.004	:	
7889.90	[Ni III]	1F		e
7959.70	N I		7959.75	0.010	0.004	:	c
8116	He I	4/16	8116.39	0.015	0.006	39	
8203.85	He I	4/14	8203.78	0.021	0.008	27	
8216.28	N I	2	8216.15	0.093	0.037	7	
8223.14	N I	2	8222.96	0.102	0.041	7	
8245.64	H I	P42	8245.58	0.102	0.041	7	
8247.73	H I	P41	8247.70	0.117	0.047	6	
8249.97	H I	P40	8249.89	0.117	0.047	6	
8252.40	H I	P39	8252.31	0.123	0.049	6	
8255.02	H I	P38	8254.93	0.124	0.049	6	
8257.85	H I	P37	8257.92	0.093	0.037	7	
8260.93	H I	P36	8260.98	0.105	0.041	6	
8263.82	Fe I		8263.76	0.023	0.009	25	c
8264.28	H I	P35	8264.41	0.115	0.047	7	
8267.94	H I	P34	8267.86	0.169	0.067	5	
8271.93	H I	P33	8271.85	0.184	0.073	5	
8276.31	H I	P32	8276.26	0.195	0.077	5	g
8281.12	H I	P31	8281.01	0.160	0.063	5	e
8286.43	H I	P30	8286.31	0.214	0.084	5	e
8292.31	H I	P29	8292.25	0.271	0.106	4	e
8298.83	H I	P28	8298.72	0.272	0.107	4	e
8306.11	H I	P27	8306.25	0.132	0.052	6	
8314.26	H I	P26	8314.14	0.334	0.131	4	
8323.42	H I	P25	8323.36	0.386	0.151	4	
8333.78	H I	P24	8333.70	0.375	0.146	4	
8342.33	He I	4/12	8342.22	0.020	0.008	28	
8345.55	H I	P23	8345.44	1.643	0.638	4	e
8359.00	H I	P22	8358.93	0.545	0.211	4	
8361.67	He I	1/6	8361.65	0.211	0.082	5	
8374.48	H I	P21	8374.38	0.519	0.200	4	
8387.77	Fe I		8387.48	0.010	0.004	:	c
8392.40	H I	P20	8392.31	0.707	0.272	4	
8397.	He I	6/19	8397.31	0.016	0.006	36	
8413.32	H I	P19	8413.24	0.808	0.309	4	
8422.	He I	6/18	8421.91	0.021	0.008	28	
8437.96	H I	P18	8437.88	0.913	0.347	4	
8444.34	He I	4/11	8444.42	0.051	0.019	12	
8446.25	O I	4	8446.34	0.809	0.307	4	e
8446.36	O I	4					
8446.76	O I	4	8446.71	0.333	0.126	4	
8451.00	He I	6/17	8451.10	0.027	0.010	22	
8459.32	[Cr II]		8459.17	0.025	0.010	22	
8467.25	H I	P17	8467.19	1.031	0.390	4	
8480.90	[Cl III]	3F	8480.77	0.012	0.005	:	

TABLE 2 (CONTINUED)

λ_0 (Å)	Ion	Mult.	λ_{obs} (Å)	$F(\lambda)$	$I(\lambda)^a$	err (%) ^b	Notes
8486.	He I	6/16	8486.23	0.037	0.014	15	
8488.	He I	7/16	8488.67	0.013	0.005	:	
8500.00	[Cl III]	3F	8499.74	0.045	0.017	13	
8502.48	H I	P16	8502.40	1.302	0.488	4	
8518.04	He I	2/8	8517.93	0.027	0.010	22	
8528.99	He I	6/15	8528.98	0.043	0.016	14	
8665.02	H I	P13	8664.94	2.443	0.885	4	
8680.28	N I	1	8680.06	0.072	0.026	9	
8683.40	N I	1	8683.20	0.077	0.028	8	
8686.15	N I	1	8685.91	0.048	0.017	12	
8703.25	N I	1	8703.06	0.050	0.018	12	
8711.70	N I	1	8711.50	0.056	0.020	11	
8718.83	N I	1	8718.69	0.033	0.012	17	
8727.13	[C I]	3F	8726.99	0.363	0.130	4	
8728.90	[Fe III]	8F	8728.78	0.014	0.005	:	
8728.90	N I	28					
8733.43	He I	6/12	8733.37	0.080	0.029	8	
8736.04	He I	7/12	8735.98	0.023	0.008	25	
8750.47	H I	P12	8750.40	3.075	1.094	4	
8816.82	He I	10/12	8816.57	0.014	0.005	:	
8829.40	[S III]	3F	8829.62	0.030	0.011	19	
8845.38	He I	6/11	8845.33	0.118	0.041	6	
8848.05	He I	7/11	8847.95	0.036	0.013	16	
8862.79	H I	P11	8862.71	4.110	1.429	4	
8889.00	C II]		8888.68	0.015	0.005	38	c
8891.91	[Fe II]	13F	8891.84	0.034	0.012	17	
8894.07	Fe I]		8893.69	0.031	0.011	18	c
8914.77	He I	2/7	8914.68	0.035	0.012	16	
8946.05	Fe II]		8946.03	0.017	0.006	34	c
8996.99	He I	6/10	8996.90	0.142	0.048	6	
8999.40	He I	7/10	8999.63	0.023	0.008	25	
9014.91	H I	P10	9014.85	5.246	1.770	4	
9019.19	Fe I		9019.30	0.011	0.004	:	c
9029.30	C II		9029.11	0.032	0.011	19	c
9063.29	He I	4/8	9063.13	0.053	0.018	11	
9068.90	[S III]	1F	9068.86	90.844	30.337	4	
	?		9078.13	0.022	0.007	27	
9085.13	He I	10/10	9085.29	0.029	0.010	20	
9111.81	C I	3	9111.65	0.030	0.010	20	
9113.70	Cl II]		9113.36	0.011	0.004	:	c
9123.60	[Cl II]		9123.53	0.180	0.059	5	
9204.17	O II		9203.92	0.030	0.010	19	
9210.28	He I	6/9	9210.29	0.195	0.063	5	
9213.20	He I	7/9	9213.01	0.064	0.021	10	
9226.62	[Fe II]	13F	9226.46	0.038	0.012	15	
9229.01	H I	P9	9228.92	7.367	2.388	4	
9463.57	He I	1/5	9463.62	0.209	0.065	5	
9516.57	He I	4/7	9516.46	0.151	0.047	6	
9526.16	He I	6/8	9526.42	0.049	0.015	12	
9530.60	[S III]	1F	9530.95	192.601	59.242	4	g
9545.97	H I	P8	9546.03	4.396	1.349	4	
9603.44	He I	2/6	9603.26	0.109	0.033	7	
9702.62	He I	75	9701.62	0.022	0.006	26	g
9824.13	[C I]	1F	9823.97	0.531	0.156	5	
9850.24	[C I]	1F	9849.88	1.472	0.430	4	
9903.46	C II	17.02	9903.40	0.165	0.048	6	
9903.88	C II	17.02					
10027.70	He I	6/7	10027.68	0.557	0.159	5	
10031.20	He I	7/7	10031.13	0.182	0.052	5	
10049.37	H I	P7	10049.30	20.379	5.783	5	
10286.70	[S II]	3F	10286.40	2.545	0.699	5	
10320.49	[S II]	3F	10320.31	1.645	0.449	5	
10336.41	[S II]	3F	10336.22	1.223	0.333	5	

TABLE 2 (CONTINUED)

λ_0 (Å)	Ion	Mult.	λ_{obs} (Å)	$F(\lambda)$	$I(\lambda)^a$	err (%) ^b	Notes
10340.83	O I		10341.22	0.237	0.065	5	
10370.50	[S II]	3F	10370.38	0.688	0.187	5	
M 17							
3187.84	He I	3	3187.82	0.820	2.610	30	
3587.28	He I	32	3587.30	0.120	0.266	:	
3613.64	He I	6	3613.72	0.215	0.465	25	
3634.25	He I	28	3634.38	0.236	0.504	23	
3663.40	H I	H29	3663.40	0.123	0.258	:	
3664.68	H I	H28	3664.86	0.135	0.281	37	
3666.10	H I	H27	3666.17	0.182	0.378	29	
3667.68	H I	H26	3667.83	0.162	0.337	32	
3669.47	H I	H25	3669.57	0.233	0.484	23	
3671.48	H I	H24	3671.55	0.259	0.537	21	
3673.76	H I	H23	3673.82	0.259	0.537	21	
3676.37	H I	H22	3676.46	0.310	0.641	18	
3679.36	H I	H21	3679.43	0.312	0.644	18	
3682.81	H I	H20	3682.90	0.379	0.780	16	
3686.83	H I	H19	3686.90	0.324	0.665	18	
3691.56	H I	H18	3691.63	0.453	0.927	14	
3697.15	H I	H17	3697.24	0.580	1.182	11	
3703.86	H I	H16	3703.92	0.543	1.095	12	
3705.04	He I	25	3705.11	0.338	0.682	17	
3711.97	H I	H15	3712.05	0.677	1.361	10	
3721.83	[S III]	2F	3721.94	1.307	2.609	6	
3721.94	H I	H14					
3726.03	[O II]	1F	3726.15	22.887	45.554	4	
3728.82	[O II]	1F	3728.90	23.271	46.238	4	
3734.37	H I	H13	3734.46	1.246	2.467	7	
3750.15	H I	H12	3750.23	1.579	3.095	6	
3770.63	H I	H11	3770.71	2.005	3.881	5	
3797.90	H I	H10	3797.98	2.784	5.300	4	
3819.61	He I	20	3819.70	0.678	1.273	10	
3835.39	H I	H9	3835.47	3.937	7.327	4	
3856.02	Si II	1	3856.15	0.073	0.135	20	
3856.13	O II	12					
3862.59	Si II	1	3862.71	0.084	0.155	18	
3867.48	He I	20	3867.56	0.072	0.131	21	
3868.75	[Ne III]	1F	3868.84	10.383	18.955	3	
3871.60	He I	60	3871.86	0.068	0.124	21	
3887.40	S II		3887.72	0.049	0.088	27	g
3888.65	He I	2	3889.00	9.822	17.726	3	
3889.05	H I	H8					
3918.98	C II	4	3919.07	0.024	0.043	:	
3920.68	C II	4	3920.78	0.048	0.086	27	
3926.53	He I	58	3926.65	0.070	0.123	21	
3964.73	He I	5	3964.82	0.555	0.960	5	
3967.46	[Ne III]	1F	3967.54	3.222	5.562	4	
3970.07	H I	H7	3970.16	9.053	15.605	3	
4009.22	He I	55	4009.37	0.132	0.222	13	
4026.08	N II	40	4026.30	1.362	2.269	4	
4026.21	He I	18					
4068.60	[S II]	1F	4068.74	0.263	0.427	8	
4069.62	O II	10	4069.85	0.117	0.190	14	
4069.89	O II	10					
4072.15	O II	10	4072.26	0.056	0.091	24	
4075.86	O II	10	4075.99	0.054	0.087	25	
4076.35	[S II]	1F	4076.50	0.081	0.131	19	
4097.22	O II	20	4097.38	0.040	0.064	31	
4097.26	O II	48					
4100.62	D I	D6	4100.75	0.018	0.028	:	
4101.74	H I	H6	4101.83	0.015	23.920	3	
4120.84	He I	16	4120.91	0.136	0.213	13	

TABLE 2 (CONTINUED)

λ_0 (Å)	Ion	Mult.	λ_{obs} (Å)	$F(\lambda)$	$I(\lambda)^a$	err (%) ^b	Notes
4143.76	He I	53	4143.84	0.174	0.270	11	
4153.30	O II	19	4153.41	0.060	0.093	23	
4168.97	He I	52	4169.11	0.057	0.087	24	
4169.22	O II	19					
4267.15	C II	6	4267.26	0.396	0.580	6	
4303.61	O II	66	4303.93	0.046	0.066	29	
4303.82	O II	53					
4317.14	O II	2	4317.34	0.042	0.061	30	
4319.63	O II	2	4319.77	0.027	0.037	:	
4339.29	D I	D5	4339.42	0.017	0.024	:	
4340.47	H I	H5	4340.56	32.184	45.582	3	
4345.55	O II	65c	4345.67	0.062	0.088	23	
4345.56	O II	2					
4349.43	O II	2	4349.62	0.047	0.066	28	
4363.21	[O III]	2F	4363.29	0.682	0.953	5	
4366.89	O II	2	4366.99	0.021	0.030	:	
4368.15	O I	5	4368.64	0.016	0.022	:	
4368.25	O I	5					
4387.93	He I	51	4388.03	0.420	0.578	6	
4437.55	He I	50	4437.69	0.055	0.073	25	
4471.48	He I	14	4471.60	3.653	4.733	3	
4491.07	C II		4491.39	0.028	0.036	:	
4491.23	O II	86a					
4607.06	[Fe III]	3F	4607.19	0.029	0.034	:	
4607.16	N II	5					
4609.44	O II	93	4609.50	0.017	0.020	:	
4621.39	N II	5	4621.60	0.016	0.019	:	
4630.54	N II	5	4630.69	0.048	0.055	28	
4638.86	O II	1	4638.95	0.081	0.093	19	
4640.64	N III	2	4640.83	0.021	0.024	:	
4641.81	O II	1	4641.97	0.111	0.128	15	
4643.06	N II	5	4643.35	0.019	0.022	:	
4649.13	O II	1	4649.26	0.107	0.123	15	
4650.84	O II	1	4650.95	0.087	0.100	18	
4658.10	[Fe III]	3F	4658.23	0.239	0.273	9	
4661.63	O II	1	4661.73	0.105	0.119	15	
4673.73	O II	1	4673.80	0.020	0.022	:	
4676.24	O II	1	4676.36	0.039	0.044	32	
4701.62	[Fe III]	3F	4701.70	0.063	0.069	23	
4711.37	[Ar IV]	1F	4711.52	0.040	0.044	32	
4713.14	He I	12	4713.29	0.448	0.493	6	
4733.91	[Fe III]	3F	4734.10	0.012	0.013	:	
4740.16	[Ar IV]	1F	4740.30	0.021	0.023	:	
4754.83	[Fe III]	3F	4754.87	0.041	0.044	31	
4769.60	[Fe III]	3F	4769.64	0.030	0.032	39	
4777.78	[Fe III]	3F	4777.99	0.020	0.021	:	
4802.23	C II		4802.55	0.031	0.032	38	
4860.03	D I	D4	4860.18	0.042	0.042	31	
4861.33	H I	H4	4861.44	100.000	100.000	3	
4881.00	[Fe III]	2F	4881.10	0.083	0.082	20	
4921.93	He I	48	4922.04	1.293	1.243	3	
4924.50	[Fe III]	2F	4924.72	0.060	0.057	23	
4924.50	O II	28					
4931.32	[O III]	1F	4931.36	0.063	0.060	22	
	[O III]	blue comp	4957.81	0.058	0.055	23	
4958.91	[O III]	1F	4959.03	121.424	114.066	3	
	[O III]	blue comp	5005.81	0.170	0.156	9	
5006.84	[O III]	1F	5007.06	367.706	335.383	3	
5015.68	He I	4	5015.88	2.609	2.368	3	
5041.03	Si II	5	5041.25	0.127	0.114	11	
5047.74	He I	47	5047.94	0.133	0.119	11	
5055.98	Si II	5	5056.27	0.121	0.107	12	
5191.82	[Ar III]	1F	5191.87	0.072	0.059	17	

TABLE 2 (CONTINUED)

λ_0 (Å)	Ion	Mult.	λ_{obs} (Å)	$F(\lambda)$	$I(\lambda)^a$	err (%) ^b	Notes
5197.90	[N I]	1F	5198.41	0.225	0.184	8	
5200.26	[N I]	1F	5200.79	0.151	0.123	10	
5270.30	[Fe III]	1F	5270.74	0.172	0.136	9	
5517.71	[Cl III]	1F	5517.86	0.721	0.496	5	
5537.88	[Cl III]	1F	5538.03	0.532	0.362	5	
5666.64	N II	3	5666.83	0.060	0.038	19	
5679.56	N II	3	5679.78	0.125	0.078	12	
5710.76	N II	3	5711.00	0.020	0.012	39	
5754.64	[N II]	3F	5754.85	0.439	0.262	6	
5875.64	He I	11	5875.82	24.069	13.446	3	
5931.79	N II	28	5932.01	0.056	0.031	20	
5957.56	Si II	4	5957.70	0.049	0.026	22	
5978.83	Si II	4	5979.16	0.074	0.039	16	
6151.27	C II	16.04	6151.57	0.036	0.018	27	
6151.54	C II	16.04					
6300.30	[O I]	1F	6300.92	5.112	2.372	4	
6312.10	[S III]	3F	6312.23	2.605	1.203	4	
6347.11	Si II	2	6347.33	0.244	0.111	8	
6363.78	[O I]	1F	6364.40	1.687	0.763	4	
6371.36	Si II	2	6371.57	0.214	0.097	9	
6461.95	C II	17.04	6462.06	0.114	0.050	13	
6462.13	C II	17.04					
6548.03	[N II]	1F	6548.33	18.064	7.604	4	
6561.04	D I	D3	6561.25	0.264	0.111	9	
6562.82	H I	H3	6562.97	681.427	285.306	4	
6578.05	C II	2	6578.16	0.861	0.359	5	
6583.41	[N II]	1F	6583.69	58.850	24.453	4	
6678.15	He I	46	6678.32	9.820	3.946	4	
6716.47	[S II]	2F	6716.70	11.462	4.546	5	
6730.85	[S II]	2F	6731.09	11.040	4.356	5	
7002.23	O I	21	7002.44	0.025	0.009	:	
7062.26	He I	1/11	7062.60	0.035	0.013	:	
7065.28	He I	10	7065.41	9.906	3.529	5	
	[Ar III]	blue comp	7134.13	0.043	0.015	:	
7135.78	[Ar III]	1F	7135.94	38.612	13.482	5	
7155.14	[Fe II]	14F	7155.48	0.025	0.009	:	
7160.58	He I	1/10	7160.73	0.055	0.019	31	
7231.34	C II	3	7231.50	0.378	0.129	7	
7236.19	C II	3	7236.54	0.567	0.192	6	
7281.35	He I	45	7281.55	1.757	0.589	5	
7298.05	He I	1/9	7298.19	0.077	0.026	23	
7318.39	[O II]	2F	7319.20	0.532	0.177	6	
7319.99	[O II]	2F	7320.35	2.824	0.936	5	
7329.66	[O II]	2F	7329.88	1.894	0.626	5	
7330.73	[O II]	2F	7330.97	1.518	0.502	5	
7377.83	[Ni II]	2F	7378.22	0.032	0.010	:	
7411.61	[Ni II]	2F	7412.49	0.022	0.007	:	
7423.64	N I	3	7423.92	0.019	0.007	:	
7442.30	N I	3	7442.85	0.027	0.009	:	
7468.31	N I	3	7468.79	0.039	0.012	:	
7499.85	He I	1/8	7500.06	0.119	0.038	16	
	[Ar III]	blue comp	7749.24	0.009	0.003	:	
7751.10	[Ar III]	2F	7751.30	12.477	3.710	5	
7771.94	O I	1	7772.13	0.084	0.025	21	e
7816.13	He I	1/7	7816.33	0.217	0.064	10	
8045.63	[Cl IV]	1F	8045.89	0.039	0.011	:	
8057.	He I	4/18	8057.78	0.023	0.007	:	
8203.85	He I	4/14	8204.05	0.050	0.013	34	
8216.28	N I	2	8216.85	0.040	0.011	:	
8255.02	H I	P38	8255.28	0.214	0.057	10	
8257.85	H I	P37	8258.14	0.191	0.051	11	
8260.93	H I	P36	8261.21	0.216	0.057	10	
8264.28	H I	P35	8264.68	0.208	0.055	11	

TABLE 2 (CONTINUED)

λ_0 (Å)	Ion	Mult.	λ_{obs} (Å)	$F(\lambda)$	$I(\lambda)^a$	err (%) ^b	Notes
8265.71	He I	2/9	8265.90	0.038	0.010	:	
8267.94	H I	P34	8268.15	0.255	0.067	9	
8271.93	H I	P33	8272.09	0.239	0.063	10	
8276.31	H I	P32	8276.52	0.298	0.079	9	
8281.12	H I	P31	8281.11	0.275	0.073	9	
8286.43	H I	P30	8286.61	0.334	0.088	8	
8292.31	H I	P29	8292.54	0.401	0.106	8	
8298.83	H I	P28	8299.05	0.434	0.114	7	
8306.11	H I	P27	8306.44	0.306	0.080	8	
8314.26	H I	P26	8314.45	0.440	0.115	7	
8323.42	H I	P25	8323.64	0.545	0.142	7	
8333.78	H I	P24	8333.97	0.553	0.144	7	
8342.33	He I	4/12	8342.50	0.047	0.012	35	
8345.55	H I	P23	8345.44	4.026	1.042	6	e
8359.00	H I	P22	8359.22	0.851	0.219	6	
8361.67	He I	1/6	8361.89	0.420	0.108	8	
8374.48	H I	P21	8374.71	0.813	0.208	7	
8392.40	H I	P20	8392.61	1.078	0.274	6	
8397.	He I	6/19	8397.55	0.042	0.011	:	
8413.32	H I	P19	8413.54	1.261	0.318	6	
8422.	He I	6/18	8422.16	0.044	0.011	38	
8437.96	H I	P18	8438.17	1.424	0.355	6	
8444.34	He I	4/11	8444.68	0.094	0.023	19	
8446.25	O I	4	8447.02	0.627	0.156	7	
8446.36	O I	4					
8446.76	O I	4					
8451.00	He I	6/17	8451.48	0.064	0.016	27	
8467.25	H I	P17	8467.49	1.659	0.409	6	
8486.	He I	6/16	8486.51	0.077	0.019	23	
8502.48	H I	P16	8502.70	2.078	0.504	6	
8518.04	He I	2/8	8518.33	0.067	0.016	26	
8528.99	He I	6/15	8529.28	0.101	0.024	18	
8665.02	H I	P13	8665.20	4.065	0.919	7	e
8680.28	N I	1	8680.92	0.125	0.028	15	
8683.40	N I	1	8683.91	0.051	0.012	33	
8703.25	N I	1	8703.76	0.026	0.006	:	
8711.70	N I	1	8712.28	0.032	0.007	:	
8718.83	N I	1	8719.36	0.022	0.005	:	
8733.43	He I	6/12	8733.66	0.187	0.041	12	
8736.04	He I	7/12	8736.26	0.055	0.012	31	
8750.47	H I	P12	8750.71	5.344	1.165	7	
8776.77	He I	4/9	8777.04	1.182	0.255	7	
8816.82	He I	10/12	8816.82	0.032	0.007	:	
8829.40	[S III]	3F	8829.92	0.033	0.007	:	
8845.38	He I	6/11	8845.74	0.347	0.073	9	
8848.05	He I	7/11	8848.22	0.107	0.022	18	
8854.11	He I	5/11	8854.52	0.043	0.009	39	
8862.79	H I	P11	8863.03	7.237	1.509	7	
8996.99	He I	6/10	8997.20	0.361	0.072	9	
8999.40	He I	7/10	8999.91	0.085	0.017	21	
9014.91	H I	P10	9015.16	9.624	1.906	7	
9063.29	He I	4/8	9063.54	0.230	0.045	11	
	[S III]	blue comp	9066.78	0.117	0.023	18	
9068.90	[S III]	1F	9069.13	159.709	31.157	7	
9085.13	He I	10/10	9085.52	0.054	0.010	32	
9123.60	[Cl II]		9123.97	0.085	0.016	21	
9210.28	He I	6/9	9210.58	0.509	0.096	8	
9213.20	He I	7/9	9213.26	0.111	0.021	17	
9229.01	H I	P9	9229.24	13.208	2.492	7	
9516.57	He I	4/7	9516.68	0.327	0.060	9	
9526.16	He I	6/8	9526.64	0.386	0.071	9	
	[S III]	blue comp	9528.81	0.056	0.010	:	
9530.60	[S III]	1F	9531.23	429.095	78.661	7	

TABLE 2 (CONTINUED)

λ_0 (Å)	Ion	Mult.	λ_{obs} (Å)	$F(\lambda)$	$I(\lambda)^a$	err (%) ^b	Notes
9545.97	H I	P8	9546.21	10.487	1.921	7	
9603.44	He I	2/6	9603.59	0.168	0.031	13	
9824.13	[C I]	1F	9824.66	0.086	0.016	21	
9850.24	[C I]	1F	9850.65	0.246	0.045	10	
9903.46	C II	17.02	9903.77	1.002	0.183	8	d
9903.88	C II	17.02					
10027.70	He I	6/7	10027.97	1.526	0.279	7	
10031.20	He I	7/7	10031.43	0.474	0.087	8	
10049.37	H I	P7	10049.65	38.832	7.110	7	
10310.70	He I	4/6	10310.82	2.952	0.541	7	
10320.49	[S II]	3F	10320.92	0.756	0.139	8	
10336.41	[S II]	3F	10336.89	0.604	0.111	8	

^aFor M8, $c(\text{H}\beta)=0.94$ and $I(\text{H}\beta)=2.543 \times 10^{-11}$ ergs cm⁻² s⁻¹). For M17, $c(\text{H}\beta)=1.17$ and $I(\text{H}\beta)=1.201 \times 10^{-11}$ ergs cm⁻² s⁻¹).

^bColons indicate uncertainties larger than 40%.

^cDubious identification.

^dBlend with an unknown line.

^eAffected by telluric emission lines.

^fAffected by internal reflections or charge transfer in the CCD.

^gAffected by atmospheric absorption bands.

ing García-Rojas et al. (2004), adding quadratically the error due to flux calibration, that has been assumed as 3%, as estimated in García-Rojas et al. (2006) for similar data taken with the same instrumentation, and for which there were additional standard stars. Fractional error in the line fluxes relative to $\text{H}\beta$, $F(\lambda)$, can be estimated taking into account that fractional errors in Column seven were computed by propagating the uncertainty in the extinction correction.

A total of 375 and 260 emission lines were measured in M8 and M17, respectively. Most of the lines are permitted. We have measured 97 forbidden lines in M8, and 52 in M17. We have detected also 5 semiforbidden lines in M8. Several lines were strongly affected by atmospheric absorption features or by charge transfer in the CCD, rendering their intensities unreliable. Also, some lines are dubious identifications and 3 emission lines in M8 could not be identified in any of the available references. All those lines are indicated in Table 2.

The identification and adopted laboratory wavelengths of the lines were obtained following previous identifications in the literature (see Esteban et al. 2004; García-Rojas et al. 2004, and references therein). Several previously unidentified lines in M8 (EPTGR) have been identified (see Table 2). Lines unidentified by EPTGR in M8 which are not in our line list are probably telluric emission lines or nebular lines which were severely blended with telluric lines. In particular, the features at 5865.15 Å, 6863.45 Å, and 8833.17 Å were identified by Oster-

brock et al. (1996) as OH night-sky lines. We have identified $\lambda 10021.05$ Å line as a telluric line. Also, the two lines not identified by EPTG in position 14 of M17 have been identified here as He I $\lambda\lambda 7160.58$ (1/10), 8486 (6/16).

It is known that the main ionization source for the hourglass nebula in M8 is the star H36, and that it shows a considerably higher extinction than other zones of M8. For H36, the $A_v/E(B-V)$ ratio, R , has been determined as 4.6 by Hecht et al. (1982) and as 5.3 by Cardelli, Clayton, & Mathis (1989). Following Sánchez & Peimbert (1991) and Peimbert et al. (1993) we have adopted for this zone of M8 a reddening function with $R_v = 5.0$ parametrized by Cardelli et al. (1989) for $\lambda \geq 4100$ Å. A reddening coefficient of $c(\text{H}\beta) = 0.94 \pm 0.03$ was derived. This value is intermediate between $c(\text{H}\beta) = 0.85 \pm 0.05$ obtained by EPTGR and $c(\text{H}\beta) = 1.00 \pm 0.10$ derived by Sánchez & Peimbert (1991) and Peimbert et al. (1993) for the same slit position. For the reddening function assumed for $\lambda < 4100$ Å see § 3.1.

For M17, we have adopted the standard extinction for the Milky Way parametrized by Seaton (1979). We have obtained a reddening coefficient of $c(\text{H}\beta) = 1.17 \pm 0.05$, which is also intermediate between the values obtained by EPTG (1.05 ± 0.05) and Peimbert et al. (1992) (1.20) for the same slit position.

3.1. Extinction correction in M8 for $\lambda < 4100$ Å.

In Figure 1 we show the ratio of the observed fluxes of H I Balmer lines and He I lines measured

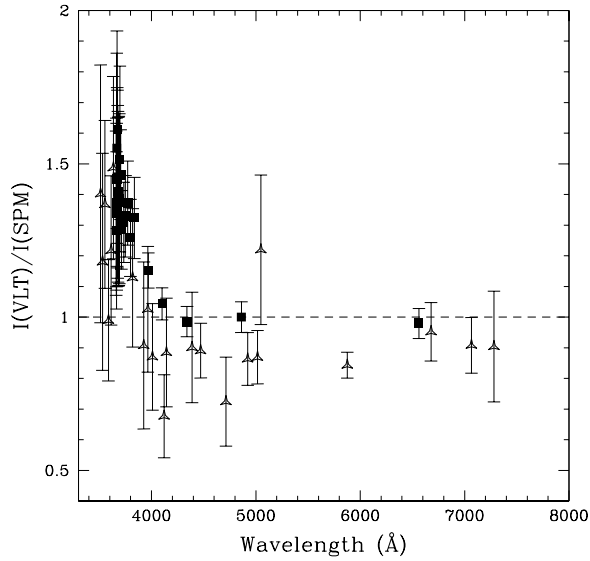


Fig. 1. Line flux ratio of H I Balmer lines (squares) and He I lines (triangles) measured in this work compared to those measured by EPTGR for M8 (see text).

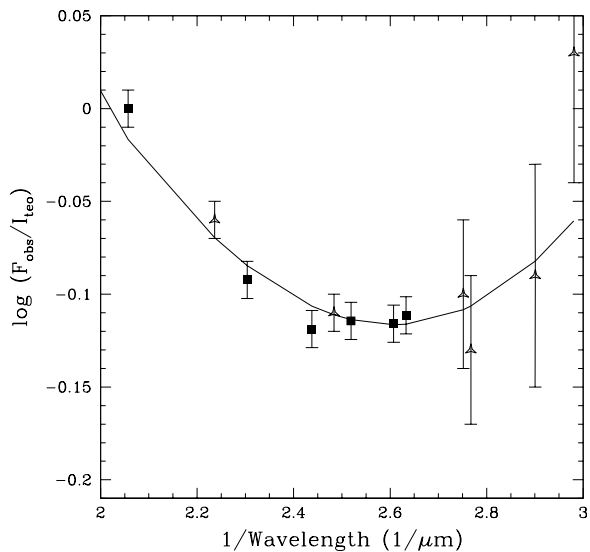


Fig. 2. Polynomial fit to the ratio of observed over theoretical fluxes of some H I Balmer lines (from H10 to H β , squares) and some He I lines (triangles). Note that for $\lambda < 4100 \text{ \AA}$ ($1/\lambda > 2.44$) the behavior of the lines is anomalous (see text).

by us and by EPTGR. It can be seen that for wavelengths shorter than 4100 \AA our line fluxes are higher than those measured by EPTGR. So if we assume the extinction correction adopted above, the intensity of these lines would be overestimated. The effect seems

to be an observational bias instead of a physical effect; actually M8 is the object that was observed at the highest air mass –sec $z \sim 2$ –, so it is possible that an unsuitable operation of the Atmospheric Dispersion Corrector (ADC) at high airmasses used on our observations caused this effect. The gradient in the reddening and in the surface brightness of the Hour-glass region is very strong and atmosphere refraction effects could include regions of higher emissivity in the blue part of the spectrum that are not included at $\lambda > 4100 \text{ \AA}$.

To correct for this effect, we have done a polynomial fit to the observed over theoretical flux ratios of H I Balmer lines and He I lines (which are in case B and are not affected by self-absorption: He I $\lambda\lambda$ 3354.55, 3447.59, 3613.64, 3634.25, 4026.08, and 4471.48) and interpolated to all wavelengths shortwards of 4100 \AA (see Figure 2). We have not included H I Balmer lines with quantum number higher than 10 in this fit due to the higher dependence of these line ratios on density (see e.g., Zhang et al. 2004). This fit is used to interpolate for all the wavelengths shortwards of 4100 \AA . The correction has not affected significantly the physical conditions and the chemical abundances derived in this work –less than 0.05 and 0.1 dex in the total abundances of O and Ne, respectively, which are the species most affected by this effect.

4. PHYSICAL CONDITIONS

4.1. Temperatures and Densities

We have derived physical conditions of the two nebulae using several emission line ratios. The temperatures and densities are presented in Table 3. The values of T_e and n_e were derived using the IRAF task *temden* of the package *nebular* (Shaw & Dufour 1995) with updated atomic data (see García-Rojas et al. 2005), except in the case of the n_e derived from [Fe III] lines. We have derived the [Fe III] density from the intensity of the brightest lines –those with errors smaller than 30% and that do not seem to be affected by line blending, which are 14 in the case of M8 and 5 in the case of M17– together with the computations of Rodríguez (2002), following the procedure described by García-Rojas et al. (2006).

We have derived a weighted mean of $n_e(\text{O II})$, $n_e(\text{S II})$, $n_e(\text{Cl III})$, and $n_e(\text{Fe III})$ assuming an initial temperature of $T_e = 10000 \text{ K}$, then we have used this density to compute the temperatures, and iterated until convergence. The adopted n_e values are shown in Table 3. We have excluded $n_e(\text{N I})$ from the average because this ion is representative of the very outer part of the nebula, and it does not coexist with the other ions.

TABLE 3
PLASMA DIAGNOSTIC

Parameter	Line	Value	
		M8	M17
N _e (cm ⁻³)	[N I]	1600 ⁺⁷⁵⁰ ₋₄₇₀	1200 ⁺¹²⁵⁰ ₋₅₀₀
	[O II]	1800±800	480±150
	[S II]	1600±450	500±220
	[Fe III]	2600±1450	430 ^{+>1000} ₋₄₀₀
	[Cl III]	2100±700	270 ⁺⁶³⁰ ₋₂₇₀
N _e (adopted)	[Ar IV]	2450:	>800
		1800±350	470±120
T _e (K)	[N II]	8470±180 ^a	8950±380 ^a
	[S II]	7220±300	7100±750
	[O II]	8700±350 ^a	8750±550 ^a
T _e (low)		8500±150	8870±300
	[O III]	8090±140	8020±170
	[Ar III]	7550±420	8380±570
	[S III]	8600±300 ^b	8110±400
T _e (high)		8150±120	8050±150
He I		7650±200	7450±200
Balmer line/cont.		7100 ⁺¹²⁵⁰ ₋₁₀₀₀	...
Paschen line/cont.		7750±900	6500±1000

^aRecombination contribution on the auroral lines has been considered (see text).

^b[S III] λ 9530 affected by atmospheric absorption bands.

Electron temperatures from forbidden lines have been derived from [O II], [O III], [N II], [S II], [S III], and [Ar III] line ratios.

We have corrected $T_e(\text{O II})$ from the contribution to $\lambda\lambda 7320+7330$ due to recombination following the formula derived by Liu et al. (2000):

$$\frac{I_R(7320 + 7330)}{I(\text{H}\beta)} = 9.36 \times (T_4)^{0.44} \times \frac{\text{O}^{++}}{\text{H}^+}, \quad (1)$$

where $T_4 = T/10^4$. Using the O^{++}/H^+ ratio derived by EPTGR in M8 and EPTG in M17 from RLs we have estimated contributions of about 2% and 20% for M8 and M17, respectively. The large contribution of recombination to the intensity of the $\lambda\lambda 7320+7330$ lines in M17 is reflected as a drop of more than 1000 K in $T_e(\text{O II})$, which reconciles the value of $T_e(\text{O II})$ with that of $T_e(\text{N II})$.

Liu et al. (2000) also give a formula for the contribution by recombination to the intensity of the [N II] λ 5755 line:

$$\frac{I_R(5755)}{I(\text{H}\beta)} = 3.19 \times (T_4)^{0.30} \times \frac{\text{N}^{++}}{\text{H}^+}. \quad (2)$$

To derive the N^{++}/H^+ ratio, needed to compute this quantity, we have assumed that N^{++}/H^+ is well represented by the subtraction of N^+/H^+ to the total

N/H ratio, assuming that the temperature fluctuations paradigm and a ionization correction factor (hereinafter ICF) lead to the correct abundances (see § 4.2).⁷ From the results of EPTGR for M8 and EPTG for M17, the contribution of recombination to the intensity of the [N II] λ 5755 line has been estimated as 1% and 6% for M8 and M17, respectively. These contributions are small and affect by less than 200 K the derived temperature.

We have also been able to derive the electron temperatures from the Balmer and Paschen discontinuities. Figure 3 shows the spectral regions near the Balmer and the Paschen limits. The discontinuities can be clearly appreciated, except in the case of the Balmer limit of M17, for which the low signal-to-noise of the continuum makes it unreliable. We have followed the same procedure as in previous papers (e.g., García-Rojas et al. 2006) to derive the temperatures. The values adopted for $T_e(\text{H I})$ are shown in Table 3. To the best of our knowledge, no previous determinations of $T_e(\text{H I})$ (Balmer and Paschen) have been derived for M17; for M8 there was a previous $T_e(\text{H I})$ determination from the Balmer discontinuity in the Hourglass by Sánchez & Peimbert (1991) which amounts to $T_e(\text{H I}) = 6600$ K, that is somewhat smaller than what has been derived here ($T_e(\text{H I}) = 7100^{+1250}_{-1000}$ K), but consistent within the errors.

Our derived $T_e(\text{H I})$ values are in good agreement with the values obtained by Reifenstein et al. (1970) from the H109 α radio recombination line, $T_e(\text{H I}) = 7300 \pm 1000$ K for M8 and 6400 ± 750 K for M17. On the other hand, the $T_e(\text{H I})$ values derived by Shaver & Goss (1970) from radio 408 MHz continuum measurements do not agree; these authors computed $T_e = 6100$ K for M8 and 7850 K for M17, which are far from the temperatures derived here.

We have derived $T_e(\text{He I})$ assuming a 2-zone ionization scheme, characterized by $T_{e\text{II+III}}$ (see Peimbert, Peimbert, & Luridiana 2002). We have derived $T_e(\text{He I})=7650 \pm 200$ K for M8, which is highly consistent with the $T_e(\text{H I})$ derived above, and $T_e(\text{He I})=7450 \pm 200$ K for M17, which is higher than $T_e(\text{H I})$.

⁷Another way to derive the N^{++}/H^+ ratio is assuming as valid the abundance obtained from N II lines of multiplet 3, which seems to be the least affected by fluorescence effects. Nonetheless, for regions with high degree of ionization, it may be incorrect to apply permitted line abundances because, as pointed out by Grandi (1976), N II permitted lines are excited mainly by resonance fluorescence, and corrections might be high. In fact, if we assume the N^{++} abundance derived from multiplet 3, the correction would be of more than 20%, implying a $T_e(\text{N II})$ 500 K lower than that has been assumed (see § 7 for additional discussion on the N II permitted lines).

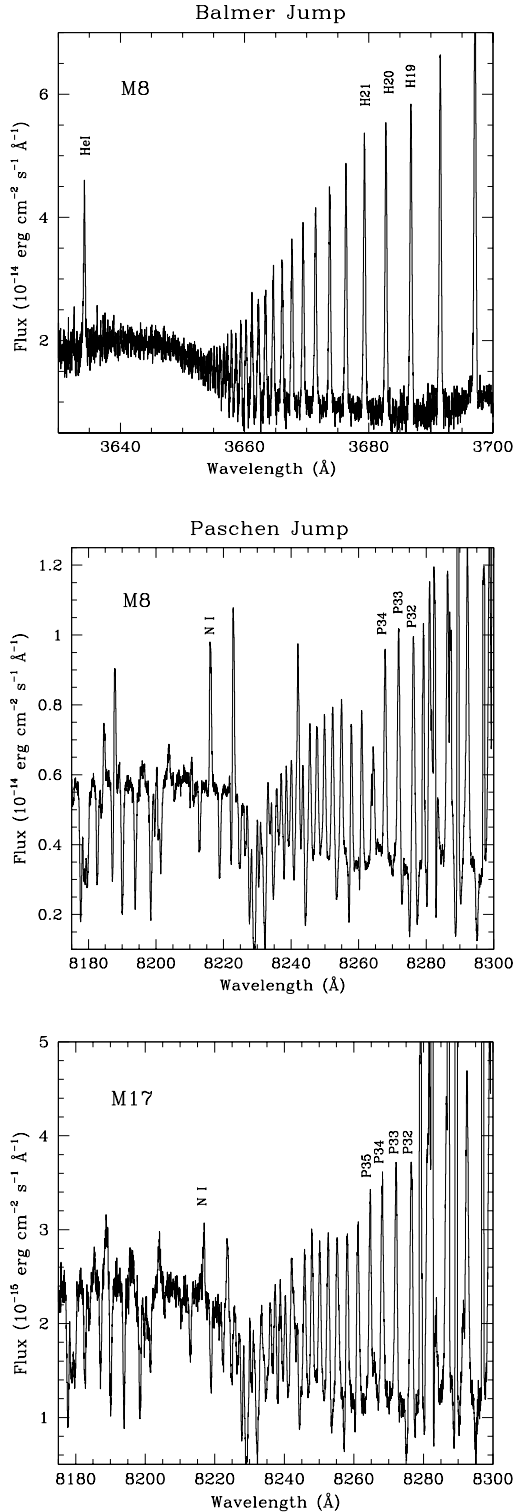


Fig. 3. Section of the echelle spectra of M8 (upper and middle panels) and M17 (lower panel) including the Balmer (upper panel) and the Paschen (middle and lower panels) limits (observed fluxes).

We have assumed a two-zone ionization scheme for all our calculations. We have adopted the average of T_e obtained from [N II] and [O II] lines as representative for the low ionization zone. We have not included $T_e(\text{S II})$ in the average because its value is much lower than those obtained from [N II] and [O II] lines. This effect has been reported previously in several objects (e.g., García-Rojas et al. 2005, 2006), and might be produced by the presence of a temperature stratification in the outer zones of the nebulae or, conversely, by errors in the atomic parameters of the ion. For the high ionization zone we have adopted the average of the values of T_e obtained from [O III], [S III] and [Ar III]. In M8 the [S III] $\lambda 9532$ line is affected by atmospheric absorption bands, so we have adopted the intensity of [S III] $\lambda 9069$ and the [S III] $\lambda 9532/\lambda 9069$ theoretical ratio to derive $T_e(\text{S III})$.

4.2. Temperature Variations

Since Torres-Peimbert et al. (1980) proposed the presence of spatial temperature fluctuations (parametrized by t^2) as a possible cause of the abundance discrepancy, many efforts have been done to find the physical processes responsible for such temperature fluctuations in H II regions (e.g., Esteban 2002; Tsamis & Péquignot 2005) and in planetary nebulae (e.g., Liu 2006; Peimbert & Peimbert 2006), but the source of temperature fluctuations and its impact on the chemical abundance determinations remain controversial topics in the study of gaseous nebulae.

Peimbert (1971) showed that there was a substantial difference between the T_e derived from the [O III] lines and the one derived from hydrogen recombination continuum discontinuities, which is strongly correlated with the abundance discrepancy (Liu et al. 2001; Tsamis et al. 2004); thus the comparison between electron temperatures derived from both methods would be an additional indicator of t^2 .

Additionally, it is also possible to derive the t^2 value from the analysis of the He I lines, because of the different temperature dependence of each of them, so we can find He I line ratios that will allow us to derive a temperature. However, in practice, each of these ratios depends simultaneously on T_0 , t^2 , n_e and τ_{3889} . Therefore, any determination must be done using several line ratios. Peimbert, Peimbert, & Ruiz (2000) developed a maximum likelihood method to search for the plasma conditions that would give the best simultaneous fit to the measured lines. In § 5 we have applied that method to our He I lines.

TABLE 4
 t^2 PARAMETER

Method	t^2	
	M8	M17
O ⁺⁺ (R/C)	0.045±0.005	0.034±0.005
O ⁺ (R/C)	0.031±0.017	0.109:
C ⁺⁺ (R/C)	0.035±0.005	...
He II	0.046±0.009	0.027±0.014
Bac/Pac-FL	0.022±0.015	0.035±0.021
Adopted	0.040±0.004	0.033±0.005

As we have assumed a two-zone ionization scheme, we have followed the formulation of Peimbert et al. (2000) and Peimbert, Peimbert, & Luridiana (2002) to derive the values of t^2 following the three methods described above.

In Table 4 we show the t^2 values derived from each method and the final adopted values, which are error-weighted averages. It is highly remarkable that all the t^2 values derived for each nebula are very consistent. The C⁺⁺/H⁺ ratio obtained from CELs for M8 has been taken from Peimbert et al. (1993), who measured the UV C II] $\lambda\lambda 1906+1909$ emission lines from IUE data. As well as when we are comparing with the infrared data (see García-Rojas et al. 2006), we cannot here discard aperture effects due to the different volumes covered by the slits in the optical and UV observations.

The t^2 values obtained in this paper are very similar to those obtained for all the bright Galactic H II regions of our sample (Esteban et al. 2004; García-Rojas et al. 2004, 2005, 2006) and are also similar to the few estimations of t^2 in extragalactic H II regions available in the literature for the Magellanic Clouds (Peimbert 2003; Tsamis et al. 2003), NGC 6822 (Peimbert et al. 2005), M101, NGC 2366, and M33 (Esteban et al. 2002) and the dwarf H II galaxy NGC 5253 (López-Sánchez et al. 2007).

A very different behavior has been found for planetary nebulae (PNe). Several authors have found a large scatter of the t^2 values determined for different PNe (see e.g., Liu 2002; Tsamis et al. 2004, and references therein). Recently, Robertson-Tessi & Garnett (2005) have found a correlation between the abundance discrepancy factor (ADF) defined by Liu et al. (2000) as $\log(\text{O}^{++}/\text{H}^+ \text{RL}) - \log(\text{O}^{++}/\text{H}^+ \text{CEL})$ and n_e . They have found that the lower n_e in the PNe, the higher ADF, with a steep slope. To illustrate the difference between both behaviors –PNe and H II regions– we have overplotted the com-

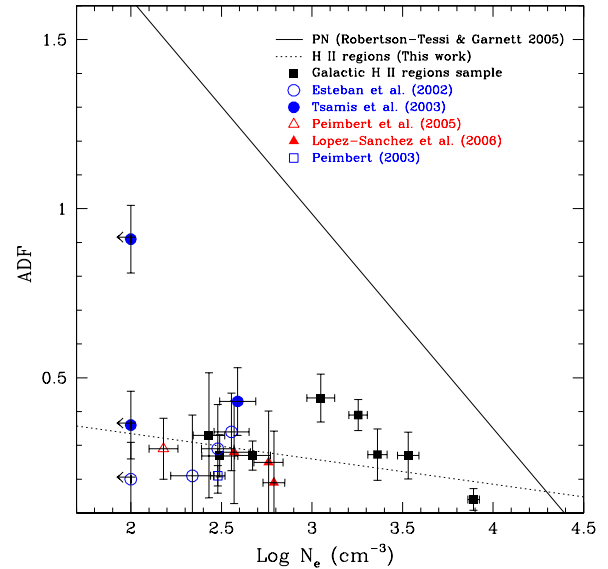


Fig. 4. Correlation between n_e and ADF for the sample of Galactic (filled squares) and extragalactic (other symbols) H II regions in which ADF has been measured. Solid line is the fit obtained by Robertson-Tessi & Garnett (2005) for a sample of PN from the literature. Dashed line is the fit obtained for H II regions.

plete set of ADFs measured in H II regions (Galactic and extragalactic) available in the literature to the Robertson-Tessi's fit ($r = -0.47$) for PNe (see Figure 4). From Figure 4 it is clear that H II regions do not follow the correlation found for PNe. In fact, it seems that there is no correlation between the H II region data, due to the similarity between the ADF values found for H II regions and to the low correlation coefficient found ($r = -0.25$). The only exception is LMC N11B, which has an ADF much larger than the other nebulae. For this object, Tsamis et al. (2003) corrected the intensity of the multiplet 1 O II lines because of the presence of absorption features, mainly caused by the presence of B stars –which have a strong O II absorption spectra– on the field covered by the slit. Nevertheless, this effect –which could be very important on extragalactic objects– can only be properly corrected if the stellar absorption features are resolved, or if stellar population synthesis spectra are available. Therefore, the O II absorption contribution can not be properly estimated using low spectral resolution data –like those used by Tsamis et al. (2003) because it is difficult to distinguish between emission and absorption features (to illustrate this point see Figure 2 of García-Rojas et al. 2006). It is not the aim of this paper to discuss more about the attenuation of the intensities of O II RLs due to

TABLE 5
HE⁺ ABUNDANCE

Line	He ⁺ /H ⁺ ^a	
	M8	M17
3819.61	673 ± 54	950 ± 95
3964.73	733 ± 59	897 ± 45
4026.21	699 ± 56	955 ± 38
4387.93	679 ± 20	918 ± 55
4471.09	662 ± 20	904 ± 27
4713.14	617 ± 19	952 ± 57
4921.93	670 ± 20	896 ± 27
5875.64	639 ± 19	880 ± 26
6678.15	666 ± 20	924 ± 37
7065.28	673 ± 20	905 ± 45
7281.35	666 ± 20	884 ± 44
Adopted ^b	662 ± 9	910 ± 14

^aIn units of 10⁻⁴, for $\tau_{3889} = 8.28 \pm 0.60$ and 7.80 ± 0.78 , and $t^2 = 0.040 \pm 0.004$ and 0.033 ± 0.005 , respectively. Uncertainties correspond to line intensity errors.

^bIt includes all the relevant uncertainties in emission line intensities, n_e , τ_{3889} and t^2 .

star absorption features, but it is important to stress that this effect should be investigated when deriving abundances from RLs in extragalactic H II regions.

5. HE⁺ ABUNDANCE

We have measured 76 and 62 He I emission lines in the spectra of M8 and M17, respectively. These lines arise mainly from recombination but they can be affected by collisional excitation and self-absorption effects. We have determined the He⁺/H⁺ ratio from a maximum likelihood method (Peimbert et al. 2000), using the n_e of Table 3 and $T(\text{O II+III}) = 8350$ K for M8, and $T(\text{O II+III}) = 8200$ K for M17 (see § 4.2). We have used the effective recombination coefficients of Storey & Hummer (1995) for H I and those of Smits (1996) and Benjamin, Skillman, & Smits (1999) for He I. The collisional contribution was estimated from the calculations made by Sawey & Berrington (1993) and Kingdon & Ferland (1995), and the optical depths in the triplet lines were derived from the computations by Benjamin, Skillman, & Smits (2002).

In Table 5 we have included the He⁺/H⁺ ratios that we have obtained for the individual He I lines not affected by line blending and with the highest signal-to-noise ratio, excluding He I $\lambda 5015$ because it could suffer self-absorption effects from the 2¹S metastable level, and $\lambda 3889$ because it is severely

blended with the H8 line. We have done a χ^2 optimization of the values in the table, and we have obtained a χ^2 parameter of 8.5 for M8 and 3.6 for M17. The values obtained indicate that the fits are good for a system with eight degrees of freedom. EPTGR, who covered a region slightly larger than ours but centered on the same location derived a He⁺/H⁺ ratio for M8–HG a factor of 1.13 (0.05 dex) higher than ours. On the other hand, Peimbert et al. (1993), who covered a similar region of the nebula, obtained a He⁺/H⁺ ratio 0.025 dex lower, confirming the strong variation with position of the values found for the He⁺/H⁺ fraction in the Hourglass in M8. For M17, the He⁺/H⁺ ratio is only a bit smaller than those obtained by EPTG (0.0975) and by Peimbert et al. (1992) (0.099); this could be due to differences in the ionization degree of the regions covered by the different slit sizes, since the O⁺⁺ abundance from RLs shows a similar behavior (see § 7).

6. IONIC ABUNDANCES FROM COLLISIONALLY EXCITED LINES

We have derived ionic abundances of N⁺, O⁺, O⁺⁺, Ne⁺⁺, S⁺, S⁺⁺, Cl⁺⁺, Cl³⁺, Ar⁺⁺ and Ar³⁺ from CELs, using the IRAF package NEBULAR. The atomic data for Cl⁺ are not implemented in NEBULAR, so we have used an old version of the five-level atom program of Shaw & Dufour (1995) (see García-Rojas et al. 2004, for more details). Ionic abundances are listed in Table 6 and correspond to the mean value of the abundances derived from all the individual lines of each observed ion, weighted by their relative intensities.

To derive the ionic abundances for $t^2 > 0.00$ we have used the abundances for $t^2 = 0.00$ and the formulation by Peimbert (1967) and Peimbert & Costero (1969). These abundances are also shown in Table 6.

Several [Fe II] lines have been detected in the spectra of M8 and M17. Unfortunately, most of them are severely affected by fluorescence effects (Rodríguez 1999a; Verner et al. 2000). One of the optical [Fe II] lines which is less affected by fluorescence effects is the [Fe II] $\lambda 8617$ line, but unfortunately it is in one of our observational gaps. However, we have measured the [Fe II] $\lambda 7155$ line, both in M8 and M17, a line which is not much affected by fluorescence effects (Verner et al. 2000). We have derived an estimation of the Fe⁺ abundance from this line, assuming that $I(\lambda 7155)/I(\lambda 8616) \sim 1$ (Rodríguez 1996) and using the calculations by Bautista & Pradhan (1996) for the emissivities of the [Fe II] $\lambda 8617$ line. We find $\text{Fe}^+/\text{H}^+ \sim 4.1 \times 10^{-8}$ for M8 and $\text{Fe}^+/\text{H}^+ \sim 1.1 \times 10^{-8}$ for M17. Nevertheless these results are

TABLE 6
IONIC ABUNDANCES FROM COLLISIONALLY EXCITED LINES^a

Ion	M8		M17	
	$t^2=0.000$	$t^2=0.040\pm 0.004$	$t^2=0.000$	$t^2=0.033\pm 0.005$
N ⁺	7.50±0.03	7.67±0.04	6.82±0.10	6.94±0.10
O ⁺	8.39±0.06	8.58±0.07	7.84±0.09	7.98±0.09
O ⁺⁺	7.86±0.03	8.18±0.07	8.41±0.04	8.67±0.06
Ne ⁺⁺	6.95±0.05	7.30±0.07	7.64±0.04	7.93±0.07
S ⁺	5.93±0.04	6.10±0.07	5.44±0.05	5.56±0.06
S ⁺⁺	6.89±0.03	7.25±0.07	6.90±0.04	7.19±0.06
Cl ⁺	4.53±0.04	4.66±0.06	3.95 ^{+0.09} _{-0.12}	4.06 ^{+0.09} _{-0.12}
Cl ⁺⁺	5.02±0.04	5.32±0.06	5.04±0.04	5.29±0.06
Cl ³⁺	3.15:	3.35:
Ar ⁺⁺	6.21±0.03	6.48±0.05	6.35±0.04	6.57±0.06
Ar ³⁺	3.69±0.09	4.01±0.10	4.15 ^{+0.12} _{-0.18}	4.42 ^{+0.13} _{-0.18}
Fe ⁺	4.61:	4.77:	4.05:	4.17:
Fe ⁺⁺	5.58±0.04	5.91±0.06	5.24±0.06	5.51±0.08

^aIn units of $12+\log(X^m/H^+)$.

TABLE 7
N⁺⁺/H⁺ RATIO FROM N II PERMITTED LINES^a

Mult.	λ_0	M8			M17		
		$I(\lambda)/I(H\beta)$ ($\times 10^{-2}$)	N ⁺⁺ /H ⁺ ($\times 10^{-5}$) ^b		$I(\lambda)/I(H\beta)$ ($\times 10^{-2}$)	N ⁺⁺ /H ⁺ ($\times 10^{-5}$) ^b	
			A	B		A	B
3	5666.64	0.027±0.004	16±2	13±2	0.038±0.007	22±4	18±3
	5676.02	0.015±0.004	18±5	15±4
	5679.56	0.034±0.004	10±1	8±1	0.078±0.009	23±3	19±2
	5686.21	0.009±0.003	17±6	14±5
	5710.76	0.010±0.003	17±5	14±4	0.012±0.005	21±8	17±7
	Sum			13±1	11±1		23±2
5	4621.39	0.022±0.004	244±54	40±9	0.019:	216:	35:
	4630.54	0.028±0.005	77±12	13±2	0.055±0.015	154±43	25±7
	4643.06	0.018±0.004	140±32	23±5	0.022:	175:	28:
	Sum			116±11	19±2		154±43
19	5001.3	0.037±0.009	8±2	8±2
20	4788.13	0.014±0.004	1447±391	28±8
	4803.29	0.011±0.004	642±214	13±4
	Sum			767±188	15±4		...
24	4994.37	0.020±0.005	700±200	30±10
28	5927.82	0.014±0.004	3892±973	46±12
	5931.79	0.020±0.004	2513±452	30±5	0.031±0.006	3889±778	46±9
	Sum			2946±410	35±5		3893±778

^aOnly lines with intensity uncertainties lower than 40% have been considered.

^bRecombination coefficients from Kisielius & Storey (2002) for cases A and B.

only an estimation, and we have marked them with colons in Table 6 due to their uncertainty.

The calculations for Fe⁺⁺ have been done with a 34-level model atom that uses collision strengths from Zhang (1996) and the transition probabilities

of Quinet (1996). We have used [Fe III] lines which do not seem affected by blends, 14 in the case of M8 and 5 in the case of M17. We have found an average value and a standard deviation of Fe⁺⁺/H⁺ = (3.78 ± 0.36) × 10⁻⁷ for M8, and Fe⁺⁺/H⁺ = (1.73 ±

$0.12) \times 10^{-7}$ for M17. Adding errors in T_e and n_e we finally obtain $12 + \log(\text{Fe}^{++}/\text{H}^+) = 5.58 \pm 0.04$ and 5.24 ± 0.06 for M8 and M17 respectively. The Fe^{++} abundances are also included in Table 6.

7. IONIC ABUNDANCES OF HEAVY ELEMENTS FROM RECOMBINATION LINES

EPTGR performed a detailed analysis of the excitation mechanisms of permitted heavy element lines in M8. In this work we have measured a large number of permitted heavy element lines, but following the study of EPTGR we have focused on the lines which are excited purely by recombination. Nevertheless, we are going to comment briefly on the N^{++}/H^+ ratio in both nebulae.

In Table 7 we show the N^{++}/H^+ ratios obtained from permitted lines in M8 and M17. Grandi (1976) argued that resonance fluorescence by the He I $\lambda 508.64$ recombination line is the dominant mechanism to excite the $4s^3P^0$ term of N II in the Orion Nebula, and hence, it should be responsible for the strengths of multiplets 3 and 5. Recently, Escalante & Morisset (2005), using tailored photoionization models of the Orion Nebula, estimate that the contribution of recombination to the intensity of multiplet 3 (which is one of the least affected by fluorescence effects of those reported in this work) is about 20% of the total intensity of the line. Additionally, we have measured a blend of two N II lines of multiplet 19 at $\lambda\lambda 5001.14, 5001.48$. These lines have upper levels $3d^3F_{2,3}^0$ that are connected to the ground state through weak dipole-allowed transitions and could have an important fluorescence contribution (Bell, Hibbert, & Stafford 1995); Escalante & Morisset (2005) predicted that recombination contributes $\sim 43\%$ to the total intensity of these two lines. Unfortunately, the only line of this multiplet which is not affected by fluorescence is the one at $\lambda 5005.15$, which is blended with the [O III] $\lambda 5007$ line. To test these theoretical predictions we have computed the N^{++} abundance from the line of multiplet 19, taking into account the contribution by fluorescence predicted by Escalante & Morisset (2005), and compared it with the N^{++} abundance estimated from the N^+ abundances assuming CELs with $t^2 > 0.00$ and the ionization correction factor for N. Also, we have proceeded in the same way with multiplet 3, taking into account that only 20% of the of the line intensities is due to recombination. In Table 8 we show the results obtained for M8 and M17 (this work), NGC 3576 (García-Rojas et al. 2004) and the Orion Nebula (Esteban et al. 2004). For the Orion Nebula and NGC 3576, we have considered

TABLE 8
COMPARISON OF N^{++}/H^+ RATIOS FROM
N II PERMITTED LINES

Mult.	$\text{N}^{++}/\text{H}^+ (\times 10^{-5})^a$			
	M8	M17	Orion	NGC 3576
3	2	8	2	2
19	3	...	3	4
$3d - 4f$	≤ 4 :	≤ 8
singlets	3:	7:
CELs ^b	4	7	6	4

^aM8 and M17: this work; Orion Nebula: Esteban et al. (2004); NGC 3576: García-Rojas et al. (2004). Colons indicate uncertainties larger than 40%.

^b N^{++} abundance obtained assuming $\text{N}/\text{H} = \text{N}^+/\text{H}^+ + \text{N}^{++}/\text{H}^{++}$, where N/H and N^+/H^+ were obtained from CELs and assuming $t^2 > 0.00$.

also $3d - 4f$ and singlet transitions, which cannot be excited by resonant fluorescence (see Grandi 1976; Escalante & Morisset 2005). In principle, there is better agreement among the abundances obtained from these lines taking into account the considerations by Escalante & Morisset (2005); nevertheless there are some puzzling results: the only $3d - 4f$ transition detected in NGC 3576 shows the larger deviation from the rest of the values, however, Escalante & Morisset (2005) proposed that there can be another mechanisms responsible for the enhancement of the intensity of these transitions, so we have to consider the abundances derived from these lines as high limits; also, from the comparison between the recombination N^{++} abundances and the values obtained from N^+/H^+ (CELs), the ICF and t^2 in Table 8 it can be seen that the agreement in M8, M17 and NGC 3576 is not very good, and that in Orion is rather poor. Nevertheless, the CELs N^{++}/H^+ ratio is very sensitive to the adopted ICF scheme, and could be reduced by as much as a factor of 2 if the adopted ICF scheme were the one of Peimbert & Costero (1969). It is clear that the measurement of pure N^{++} recombination lines (i.e. singlet transitions) could be very useful to constrain the temperature fluctuations scenario, and that much work should be done in this sense, but it is beyond the scope of this paper.

We have measured 16 permitted lines of C II in the spectrum of M8 and 13 in the spectrum of M17. Some of these lines (those of multiplets 6, 16.04, 17.02 and 17.04) are $3d - 4f$ transitions and are, in

TABLE 9
C⁺⁺/H⁺ RATIO FROM C II RECOMBINATION LINES

Mult.	λ_0	M8				M17			
		$I(\lambda)/I(H\beta)$ ($\times 10^{-2}$)	C ⁺⁺ /H ⁺ ($\times 10^{-5}$) ^a		$I(\lambda)/I(H\beta)$ ($\times 10^{-2}$)	C ⁺⁺ /H ⁺ ($\times 10^{-5}$) ^a			
			A	B		A	B		
2	6578.05	0.262 \pm 0.008 ^b	300 \pm 9	50 \pm 2	0.358 \pm 0.018	408 \pm 20	69 \pm 3		
3	7231.12	0.074 \pm 0.004	1241 \pm 67	18 \pm 1	0.129 \pm 0.009	2162 \pm 151	31 \pm 2		
	7236.19	0.112 \pm 0.004	1045 \pm 37	15 \pm 1	0.193 \pm 0.012	1800 \pm 112	26 \pm 2		
	Sum		1115 \pm 32	16 \pm 1		1929 \pm 90	27 \pm 1		
4	3918.98	0.062 \pm 0.007	1210 \pm 137	385 \pm 43	0.043 :	820 :	260 :		
	3920.68	0.133 \pm 0.008	1290 \pm 78	410 \pm 25	0.086 \pm 0.023	826 \pm 223	264 \pm 71		
	Sum		1260 \pm 68	400 \pm 22		825 \pm 200	263 \pm 62		
6	4267.26	0.222 \pm 0.009	20 \pm 1	20 \pm 1	0.580 \pm 0.035	54 \pm 3	53 \pm 3		
16.04	6151.43	0.009 \pm 0.003	21 \pm 7	...	0.018 \pm 0.005	41 \pm 11	...		
17.02	9903.43	0.048 \pm 0.003	18 \pm 1	...	0.196 \pm 0.016 ^c	68 \pm 3	...		
17.04	6461.95	0.025 \pm 0.004	22 \pm 4	...	0.050 \pm 0.007	44 \pm 6	...		
17.06	5342.38	0.011 \pm 0.004	19 \pm 7		
Adopted			20 \pm 1		48 \pm 3				

^aRecombination coefficients from Davey, Storey, & Kisielius (2000) for cases A and B.

^bAffected by telluric emission lines.

^cBlend with an unidentified line.

principle, excited by pure recombination (see Grandi 1976). In these transitions the abundances obtained are case-independent, so we have taken the mean of the values obtained for these transitions as our final adopted C⁺⁺/H⁺ ratio (the adopted lines are presented in boldface in Table 9). The result for the case-sensitive multiplet 3 gives a C⁺⁺ abundance for case B which is rather consistent with the one adopted here. We have used the effective recombination coefficients computed by Davey et al. (2000) for the abundance calculations. The dispersion of the abundances obtained from the different lines is very small, except in the case of C II λ 9903.43 line in M17, whose intensity seems to be affected by an unknown feature. The final results are in excellent agreement with those obtained by EPTGR for M8 (C⁺⁺/H⁺ = 1.9×10^{-4}) and by EPTG and Tsamis et al. (2003) for M17 (C⁺⁺/H⁺ = 4.9×10^{-4} and 4.4×10^{-4} , respectively). The complete sets of derived individual C⁺⁺/H⁺ ratios as well as the adopted one are shown in Table 9.

The O⁺ abundance was derived from the O I λ 7771.94 line, the only line of multiplet 1 that is not severely affected by telluric lines. This multiplet is case-independent and is produced mainly by recombination because it corresponds to a quintuplet transition, and the ground level is a triplet. We have also computed the O⁺/H⁺ ratio from the O I λ 8446.48 line of the multiplet 4, but Grandi (1975)

showed that starlight may contribute significantly to the observed strength of the line, which is supported by the fact that the O⁺/H⁺ ratio implied by this line is between one and two orders of magnitude larger. The effective recombination coefficients were obtained from two sources: Péquignot, Petitjean, & Boisson (1991) and Escalante & Victor (1992). Though the results are very similar, we adopted the mean of the abundances obtained with the two different coefficients. Our results are presented in Table 10. The O⁺ abundance that we have obtained for M8 is larger by a factor of 2 than that obtained by EPTGR; whereas, as pointed out below, the O⁺⁺ abundance derived from RLs is almost coincident in the two works, leading us to propose that the abundance of O⁺ derived from the O I λ 7771.96 line by EPTGR was underestimated by a factor of 2, because of the lower spectral resolution and signal-to-noise ratio of their data. The O⁺ abundance obtained for M17 from the λ 7771.94 line is very uncertain because it is partially blended with a strong sky emission line.

We have detected several O II lines in our data. Our spectra of M8 and M17 present significantly higher signal-to-noise than those published before by EPTGR and EPTG, and the number of lines to derive the O⁺⁺/H⁺ ratio has increased. The lower uncertainties and the similarity of the abundances obtained from the different lines imply that our O II

TABLE 11
O⁺⁺/H⁺ RATIO FROM O II RECOMBINATION LINES^a

Mult.	λ_0	$I(\lambda)/I(H\beta)$ ($\times 10^{-2}$)	A	O ⁺⁺ /H ⁺ ($\times 10^{-5}$) B	C
M8					
1 ^b	4638.85	0.034 ± 0.005	31 ± 4/21 ± 3	30 ± 4/20 ± 3	...
	4641.81	0.043 ± 0.005	16 ± 2/18 ± 2	16 ± 2/17 ± 2	...
	4649.14	0.041 ± 0.005	9 ± 1/13 ± 2	8 ± 1/13 ± 2	...
	4650.84	0.032 ± 0.005	31 ± 5/19 ± 2	30 ± 5/18 ± 2	...
	4661.64	0.036 ± 0.005	29 ± 4/20 ± 3	28 ± 4/19 ± 2	...
	4673.73
	4676.24	0.016 ± 0.004	18 ± 5/19 ± 4	17 ± 5/19 ± 4	...
	Sum		18 ± 1	17 ± 1	...
2	4317.14	0.011 ± 0.004	22 ± 8	16 ± 6	...
	4319.55	0.008 :	15 :	11 :	...
	4345.56 ^c	0.022 ± 0.005	41 ± 9	29 ± 6	...
	4349.43	0.020 ± 0.005	14 ± 3	10 ± 2	...
	4366.89	0.015 ± 0.004	25 ± 7	18 ± 5	...
	Sum		19 ± 3	13 ± 1	...
10 ^d	4069.62	0.067 ± 0.007	26 ± 3/26 ± 3
	4069.89				
	4072.15	0.032 ± 0.006	13 ± 2/13 ± 2
	4075.86
	Sum		20 ± 1/ 20 ± 1
15 ^e	4590.97	0.005 :	29 :	29 :	...
	Sum		29 :	29 :	...
19 ^d	4121.48	0.012 ± 0.005	1002 ± 391/746 ± 291	38 ± 15/42 ± 16	38 ± 15/40 ± 15
	4132.80	0.014 ± 0.005	626 ± 220/474 ± 166	24 ± 8/25 ± 9	24 ± 8/23 ± 8
	4153.30	0.028 ± 0.005	927 ± 176/810 ± 154	35 ± 7/35 ± 7	35 ± 7/33 ± 6
	Sum		844 ± 143/678 ± 115	32 ± 5/33 ± 6	32 ± 5/31 ± 5
3d-4f	4491.23 ^c	0.011 ± 0.004	...	70 ± 26	...
Adopted				17 ± 1	
M17					
1 ^b	4638.85	0.093 ± 0.018	85 ± 16/49 ± 9	82 ± 16/47 ± 9	...
	4641.81	0.128 ± 0.019	48 ± 7/56 ± 8	47 ± 7/54 ± 8	...
	4649.14	0.123 ± 0.018	26 ± 4/57 ± 9	25 ± 4/55 ± 8	...
	4650.84	0.100 ± 0.018	98 ± 18/48 ± 9	95 ± 17/46 ± 8	...
	4661.64	0.119 ± 0.018	97 ± 15/55 ± 8	94 ± 14/54 ± 8	...
	4673.73	0.022 :	116:/57:	112:/55:	...
	4676.24	0.044 ± 0.014	48 ± 15/55 ± 18	46 ± 15/53 ± 17	...
	Sum		53 ± 4	51 ± 4	...
2	4317.14	0.061 ± 0.018	119 ± 36	84 ± 25	...
	4319.55	0.037 :	72 :	51 :	...
	4345.56 ^c	0.088 ± 0.020	163 ± 37	116 ± 27	...
	4349.43	0.066 ± 0.018	49 ± 14	35 ± 10	...
	4366.89	0.030 :	48 :	34 :	...
	Sum		68 ± 12	48 ± 9	...
10 ^d	4069.62	0.190 ± 0.027	75 ± 11/73 ± 10
	4069.89				
	4072.15	0.091 ± 0.022	38 ± 9/38 ± 9
	4075.86	0.087 ± 0.022	25 ± 6/25 ± 6
	Sum		44 ± 5/ 43 ± 5
19 ^d	4121.48
	4132.80
	4153.30	0.092 ± 0.021	3105 ± 715/2714 ± 625	117 ± 27/118 ± 27	117 ± 27/110 ± 25
	Sum		3105 ± 715/2714 ± 625	117 ± 27/118 ± 27	117 ± 27/110 ± 25
Adopted				48 ± 2	

^aOnly lines with intensity uncertainties lower than 40% have been considered. Recombination coefficients are those of Storey (1994) for cases A and B unless otherwise stated.

^bNot corrected from NLTE effects/corrected from NLTE effects (see text).

^cBlend.

^dValues for LS coupling (Storey 1994)/intermediate coupling (Liu et al. 1995).

^eDielectronic recombination rates by Nussbaumer & Storey (1984).

TABLE 12
TOTAL GASEOUS ABUNDANCES

Element	M8		M17	
	$t^2=0.000$	$t^2=0.040\pm 0.004$	$t^2=0.000$	$t^2=0.033\pm 0.005$
He ^a	11.01±0.03	10.97±0.03	10.97±0.01	10.97±0.01
C ^b	8.61/8.69±0.09	8.70/8.69±0.09	8.77±0.04	8.77±0.04
N	7.72±0.03	7.96±0.06	7.62±0.12	7.87±0.13
O	8.51±0.05	8.73±0.05	8.52±0.04	8.76±0.05
O ^c	8.71±0.04	8.71±0.04	8.76±0.04	8.76±0.04
Ne	7.81±0.12	8.03±0.13	7.74±0.07	8.01±0.09
S	6.94±0.03	7.28±0.06	7.01±0.04	7.33±0.06
Cl ^d	5.14±0.04	5.41±0.06	5.08/5.06±0.04	5.32/5.30±0.06
Ar	6.52±0.04	6.69±0.07	6.39±0.14	6.59±0.15
Fe	5.69±0.08	6.04±0.09	5.87±0.12	6.22±0.14

^aFor M8: ICF(He) from Peimbert & Torres-Peimbert (1977).

^bFor M8: ICF from a [C II] UV line/ICF from Garnett et al (1999).

^cFor M8: O⁺⁺/H⁺ and O⁺/H⁺ from RLs. For M17: O⁺⁺/H⁺ from RLs and O⁺/H⁺ from CELs and t^2 .

^dFor M17: from Cl⁺/H⁺+Cl⁺⁺/H⁺+Cl³⁺/H⁺. For M8: ICF(Cl) from Peimbert & Torres-Peimbert (1977).

and $t^2 > 0.00$, because O⁺/H⁺ from RLs was not reliable (see § 7). In Table 12 we present the adopted total abundances for M8 and M17.

9. DETECTION OF DEUTERIUM BALMER LINES IN M8 AND M17

Hébrard et al. (2000) reported the detection of deuterium Balmer lines in the spectrum of M8, but they did not find these features in M17. In M8 these authors detected from D α to D ζ . We have detected several weak features in the blue wings of H I Balmer lines in M8 –from H α to H ϵ – and in M17 –from H α to H δ – (see Figures 6 and 7). The apparent shifts in radial velocity of these lines with respect to the H I ones are -87.6 km s^{-1} for M8 and -78.5 km s^{-1} for M17, which are similar to the isotopic shift of deuterium, -81.6 km s^{-1} .

For M8, these weak features could be discarded as high-velocity components of hydrogen following the criteria established by Hébrard et al. (2000) to identify D I lines: (a) they are narrower than the H I line, probably because D I lines arise from much colder material in the photon-dominated region (PDR); (b) there are no similar high velocity components associated to bright lines of other ions. Furthermore, the Balmer decrement of these lines follows closely the standard fluorescence models by O’Dell, Ferland, & Henney (2001) for the Orion nebula (see Table 13), indicating that fluorescence should be the main excitation mechanism of the D I lines. The difference of the apparent shift in radial velocity measured for these lines with respect to the isotopic shift of deuterium (see above) is probably due to relative motions of the gas in the photon-dominated region or

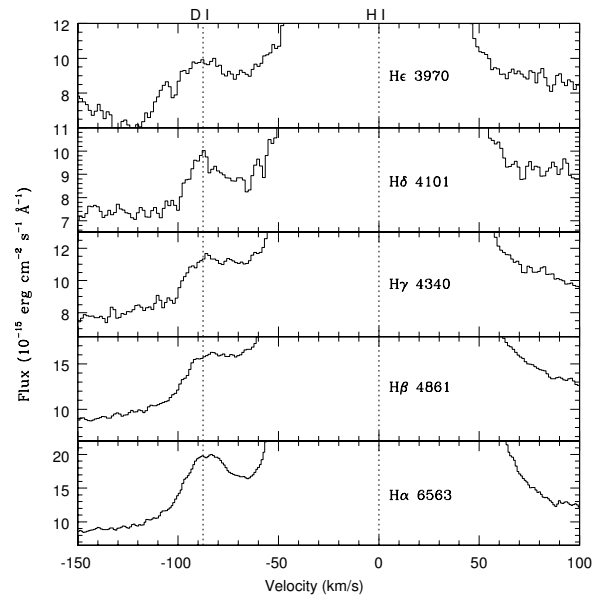


Fig. 6. Wings of H α to H ϵ in M8. The H I lines are centered at 0 km s^{-1} velocity. The dotted line of the left correspond to the average wavelength adopted for the D I lines.

PDR –where the deuterium Balmer lines are supposed to be formed– with respect to the main emitting layer of the nebula. Table 13 shows the main characteristics of the D I Balmer lines in M8.

Hébrard et al. (2000) identified the weak features in the blue wings of H I Balmer lines in M17 as high velocity components of hydrogen, mainly because of the presence of very similar features in the wings of [N II], [O II] and [O III] lines.

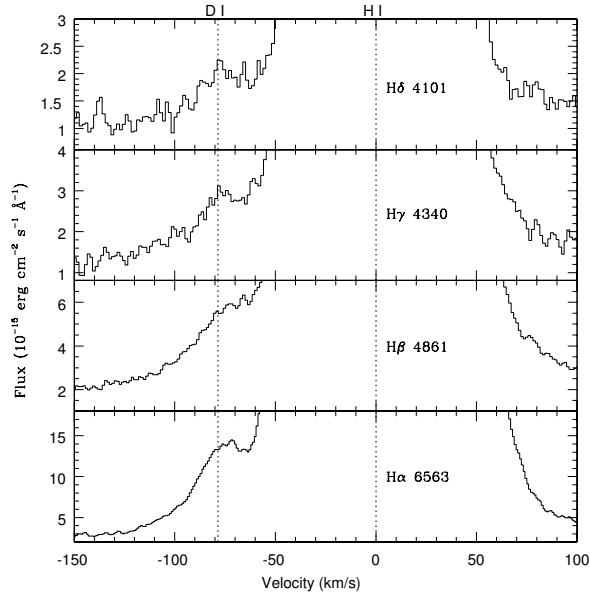


Fig. 7. Same as Figure 6, for M17. It is not clear that these features could be D I lines (see text).

TABLE 13

DEUTERIUM BALMER LINE PROPERTIES IN M8

Line	Velocity shift (km s ⁻¹)	FWHM D I (km s ⁻¹)	FWHM H I (km s ⁻¹)	D I/H I ratio (×10 ⁻⁴)
α	-87.3	< 10:	24	2.9 ± 0.2
β	-87.6	< 10:	19	3.6 ± 0.5
γ	-87.7	< 10:	19	4.1 ± 1.0
δ	-87.7	< 10:	19	6.5 ± 2.0
ε	-87.6	< 10:	19	8.8 ± 3.0

From our data we do not have a clear-cut case because: (a) the width of the H I blue-shifted feature (HBSF) is narrow, like in typical Balmer D I lines; (b) we cannot compare the ratios of HBSF/H I with the standard fluorescence models of D I Balmer lines by O’Dell et al. (2001); in principle the ratios seem to fit the model, but errors are so high that it might be possible for the HBSF/H I ratios to be constant (see Table 14); and (c) two [O III] lines $-\lambda\lambda 4959, 5007-$, two [Ar III] lines $-\lambda\lambda 7135, 7751-$ and two [S III] lines $-\lambda\lambda 9069, 9531-$ present blue counterparts at about $\sim 74, 77$ and 78 km s⁻¹ respectively, which differ by only a few km s⁻¹ from the average shift of the blue shifted H I lines (see Figure 8 [top]). These counterparts are not detected in the wings of [N II], [O II] and [S II] lines (see Figure 8 [bottom]).

Table 14 shows the main characteristics of the HBSFs in M17.

TABLE 14

H I BLUE-SHIFTED FEATURE PROPERTIES IN M17

Line	Velocity shift (km s ⁻¹)	FWHM HBSF (km s ⁻¹)	FWHM H I (km s ⁻¹)	HBSF/H I ratio (×10 ⁻⁴)
Hα	-78.6	< 10:	26	3.9 ± 0.4
Hβ	-77.7	< 10:	25	4.2 ± 1.3
Hγ	-78.7	< 10:	25	5.3 :
Hδ	-78.9	< 10:	25	11.7 :

From a simple visual inspection of Figure 8 comparing the width and central wavelength of the blue components of Hα and some forbidden lines, it is possible for the HBSFs to be a blend of D I emission and a blue-shifted high-velocity H I component, but with the available constraints we cannot guarantee it.

10. COMPARISON WITH PREVIOUS ABUNDANCE DETERMINATIONS

From the comparison of our data of M8–HGS with those published by EPTGR, it seems that a small difference in the volume covered by the slit in this zone is sufficient to change significantly the ionization degree of the gas; this fact was also pointed out by Sánchez & Peimbert (1991). This is because the emission comes from a range of densities, temperatures, degrees of ionization and sometimes extinctions within the column of gas. Nonetheless, total abundances should be invariant. In particular, the total oxygen abundance is not affected by the uncertainty of using an ICF because all the stages of ionization of this element have been detected in our optical spectra. In Table 15 we show the comparison between total abundances obtained in this work and those obtained in previous works for M8 and M17. Uncertainties reported in previous works for the total abundances are about 0.1 dex or even larger; taking into account the heterogeneity of the error criteria among the different works we have adopted errors of about 0.1 dex in this work.

The total abundances of M8 are in quite good agreement with those derived by EPTGR, within the uncertainties and taking into account that the ICFs for neon and argon (which present the largest deviations from our data) are reported as uncertain. Also, the ICF scheme and the atomic data used by EPTGR for iron are different from those used here. Making use of our atomic data and ICF scheme, the abundances obtained with the EPTGR data lead to a much better agreement (see Table 15). We have proceeded in a similar way with the data of Peim-

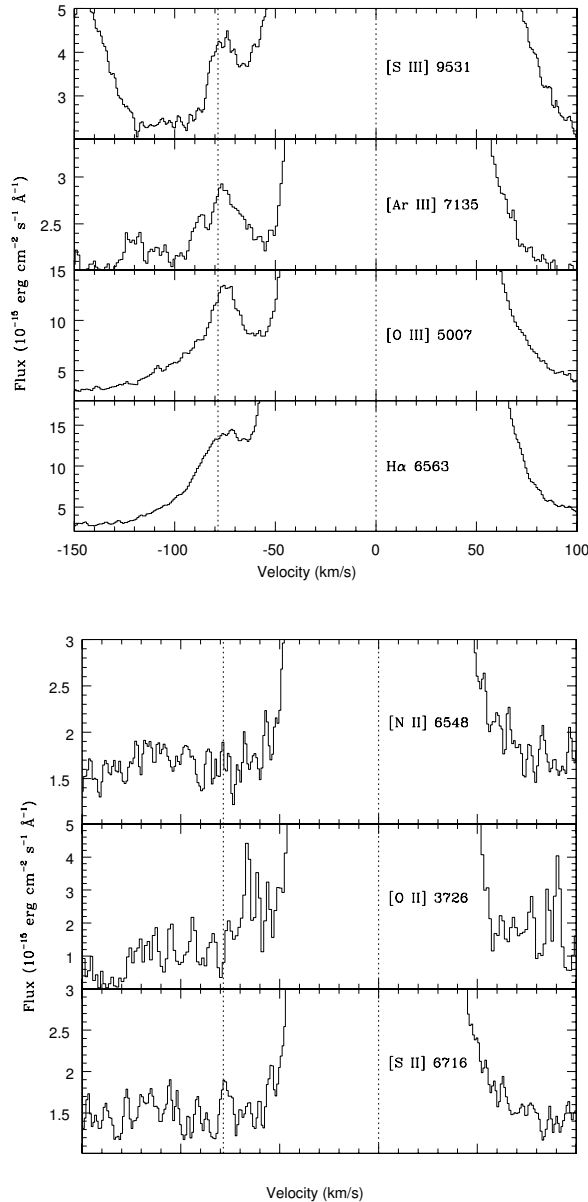


Fig. 8. Same as Figure 6, for the wings of H α , [O III] λ 5007, [Ar III] λ 7135, and [S III] λ 9531 (top) and [O II] λ 3726, [S II] λ 6716, and [N II] λ 6548 (bottom) in M17. The dotted line correspond to the average wavelength adopted for the blue-shifted H I lines.

bert et al. (1993) and Rodríguez (1999a,b), reaching the same conclusions.

The abundances of M17 are in good agreement, within the errors, with those derived by EPTG, Peimbert et al. (1992), Rodríguez (1999b) and Tsamis et al. (2003). The large differences among the different works are probably due to the different sets of atomic data and ICFs used. Proceeding in the same

way as in M8 we have recomputed the abundances for M17 using our atomic data and ICF scheme; in this case the differences with the previous calculations are of the order of 0.1 dex. Therefore, we can conclude that errors in the line intensities are not responsible for the differences among abundances of these elements by different authors (both in M8 and M17) and we emphasize the robustness of the abundances determined for these objects, bearing in mind the uncertainties due to atomic data and ICF schemes (see Table 15).

11. SUMMARY

We present new echelle spectroscopy in the 3100–10450 Å range of the Hourglass Nebula in M8 and a bright rim of M17.

We have determined the physical conditions of M8 and M17 making use of a large number of diagnostic line ratios.

We have derived ionic abundances from CELs as well as C⁺⁺/H⁺ and O⁺⁺/H⁺ ratios making use of RLs in these nebulae. The ionic abundances obtained from RLs are in very good agreement with those obtained in previous works.

The very good agreement between our results – that have been obtained making use of state-of-the-art atomic data – and the best abundance determinations from the literature for M8 and M17 allow us to conclude that the total abundances of these nebulae are very well established.

We have obtained an average t^2 of 0.040 ± 0.004 for M8 and 0.033 ± 0.005 for M17, values rather similar to those derived in previous works for these two nebulae. Also, the excellent agreement among the t^2 values obtained by independent methods is remarkable. This behavior is consistent with the temperature fluctuations scenario.

We confirm the detection of deuterium Balmer emission lines in M8 and possibly in M17, although in this case there seems to be an accidental contamination of a blueshifted high-velocity H I component.

JGR would like to thank the members of the Instituto de Astronomía, Universidad Nacional Autónoma de México, and of the Instituto Nacional de Astrofísica, Óptica y Electrónica (INAOE), for their always warm hospitality. This work has been partially funded by the Spanish Ministerio de Ciencia y Tecnología (MCyT) under project AYA2001-0436 and AYA2004-07466. MP received partial support from Conacyt (grant 46904). MR acknowledges support from Mexican Conacyt project J37680-E. MTR received partial support from FON-DAP(15010003) and Fondecyt(1010404).

TABLE 15
COMPARISON WITH PREVIOUS DETERMINATIONS^a

Element	M8				M17				
	(1)	(2)	(3)	(4) ^c	(1)	(4) ^d	(5)	(6)	(7)
N	7.72±0.03	7.68	7.75	7.60	7.62±0.12	7.50	7.59	7.55	7.57
O	8.51±0.05	8.49	8.54	8.43	8.52±0.04	8.53	8.51	8.51	8.55
Ne	7.81±0.12	7.76	7.83	...	7.74±0.07	...	7.81	7.78	7.79
S	6.94±0.03	6.96	7.03	6.95	7.01±0.04	6.99	7.03	6.84	7.05
Cl	5.14±0.04	5.21	...	5.20	5.06±0.04	5.02	5.03	5.03	5.07
Ar	6.52±0.04	6.53	6.48	6.60	6.39±0.14	6.36	6.26	6.35	6.39
Fe	5.69±0.08	5.80	...	5.72	5.87±0.12	5.75	...	5.88	...

^aIn units of 12+log(X/H). Abundances have been recomputed using our atomic data and ICF scheme (see text).

^b(1) This work; (2) EPTG; (3) Peimbert et al. (1993); (4) Rodríguez (1999a,b); (5) Tsamis et al. (2003); (6) EPTGR; (7) Peimbert et al. (1992).

^cThese data are an average of the total abundances obtained in the two slit positions located southwards of the Hourglass.

^dThese data are an average of the results obtained in three slit positions in M17.

REFERENCES

- Bautista, M. A., & Pradhan, A. K. 1996, *A&AS*, 115, 551
- Bell, K. L., Hibbert, A., & Stafford, R. P. 1995, *Phys. Scr.*, 52, 251
- Benjamin, R. A., Skillman, E. D., & Smits, D. P. 1999, *ApJ*, 514, 307
- _____. 2002, *ApJ*, 569, 288
- Cardelli, J. A., Clayton, G. C., & Mathis, J. S. 1989, *ApJ*, 345, 245
- Carigi, L., Peimbert, M., Esteban, C., & García-Rojas, J. 2005, *ApJ*, 623, 213
- Davey, A. R., Storey, P. J., & Kisielius, R. 2000, *A&AS*, 142, 85
- D’Odorico, S., Cristiani, S., Dekker, H., Hill, V., Kaufer, A., Kim, T., & Primas, F. 2000, *Proc. SPIE*, 4005, 121
- Escalante, V., & Morisset, C. 2005, *MNRAS*, 361, 813
- Escalante, V., & Victor, G. A. 1992, *Planet. Space Sci.*, 40, 1705
- Esteban, C. 2002, *RevMexAA (SC)*, 12, 56
- Esteban, C., García-Rojas, J., Peimbert, M., Peimbert, A., Ruiz, M. T., Rodríguez, M., & Carigi, L. 2005, *ApJ*, 618, L95
- Esteban, C., Peimbert, M., García-Rojas, J., Ruiz, M. T., Peimbert, A., & Rodríguez, M. 2004, *MNRAS*, 355, 229
- Esteban, C., Peimbert, M., Torres-Peimbert, S., & García-Rojas, J. 1999a, *RevMexAA*, 35, 65
- Esteban, C., Peimbert, M., Torres-Peimbert, S., García-Rojas, J., & Rodríguez, M. 1999b, *ApJS*, 120, 113
- Esteban, C., Peimbert, M., Torres-Peimbert, S., & Rodríguez, M. 2002, *ApJ*, 581, 241
- García-Rojas, J., Esteban, C., Peimbert, A., Peimbert, M., Rodríguez, M., & Ruiz, M. T. 2005, *MNRAS*, 362, 301
- García-Rojas, J., Esteban, C., Peimbert, M., Costado, M. T., Rodríguez, M., Peimbert, A., & Ruiz, M. T. 2006, *MNRAS*, 368, 253
- García-Rojas, J., Esteban, C., Peimbert, M., Rodríguez, M., Ruiz, M. T., & Peimbert, A. 2004, *ApJS*, 153, 501
- García-Rojas, J., Esteban, C., Peimbert, M., & Torres-Peimbert, S. 1998, *RevMexAA (SC)*, 7, 176
- Garnett, D. R., et al. 1999, *ApJ*, 513, 168
- Giammanco, C., & Beckman, J. E. 2005, *A&A*, 437, L11
- Grandi, S. A. 1975, *ApJ*, 196, 465
- _____. 1976, *ApJ*, 206, 658
- Hébrard, G., Péquignot, D., Walsh, J. R., Vidal-Madjar, A., & Ferlet, R. 2000, *A&A*, 364, L31
- Hecht, J., Helfer, H. L., Wolf, J., Donn, B., & Pipher, J. L. 1982, *ApJ*, 263, L39
- Howarth, I. D., & Murray, J. 1990, *SERC Starlink User Note*, No. 50
- Kingdon, J., & Ferland, G. J. 1995, *ApJ*, 442, 714
- Kisielius, R., & Storey, P. J. 2002, *A&A*, 387, 1135
- Liu, X.-W. 2002, *RevMexAA (SC)*, 12, 70
- _____. 2006, in *IAU Symp. 234, Planetary Nebulae in our Galaxy and Beyond*, ed. M. J. Barlow & R. H. Méndez (Cambridge: Cambridge Univ. Press), 219
- Liu, X.-W., Luo, S.-G., Barlow, M. J., Danziger, I. J., & Storey, P. J. 2001, *MNRAS*, 327, 141
- Liu, X.-W., Storey, P. J., Barlow, M. J., & Clegg, R. E. S. 1995, *MNRAS*, 272, 1369
- Liu, X.-W., Storey, P. J., Barlow, M. J., Danziger, I. J., Cohen, M., & Bryce, M. 2000, *MNRAS*, 312, 585
- López-Sánchez, A. R., Esteban, C., García-Rojas, J., Peimbert, M., & Rodríguez, M. 2007, *ApJ*, 656, 168
- Nussbaumer, H., & Storey, P. J. 1984, *A&AS*, 56, 293
- O’Dell, C. R., Ferland, G. J., & Henney, W. J. 2001, *ApJ*, 556, 203

- Osterbrock, D. E., Fulbright, J. P., Martel, A. R., Keane, M. J., Trager, S. C., & Basri, G. 1996, *PASP*, 108, 277
- Peimbert, A. 2003, *ApJ*, 584, 735
- Peimbert, A., Peimbert, M., & Luridiana, V. 2002, *ApJ*, 565, 668
- Peimbert, A., Peimbert, M., & Ruiz, M. T. 2005, *ApJ*, 634, 1056
- Peimbert, M. 1967, *ApJ*, 150, 825
- _____. 1971, *Boletín de los Observatorios Tonantzintla y Tacubaya*, 6, 29
- Peimbert, M., & Costero, R. 1969, *Boletín de los Observatorios Tonantzintla y Tacubaya*, 5, 3
- Peimbert, M., & Peimbert, A. 2006, in *IAU Symp. 234, Planetary Nebulae in our Galaxy and Beyond*, ed. M. J. Barlow & R. H. Méndez (Cambridge: Cambridge Univ. Press), 227
- Peimbert, M., Peimbert, A., & Ruiz, M. T. 2000, *ApJ*, 541, 688
- Peimbert, M., & Torres-Peimbert, S. 1977, *MNRAS*, 179, 217
- Peimbert, M., Torres-Peimbert, S., & Dufour, R. J. 1993, *ApJ*, 418, 760
- Peimbert, M., Torres-Peimbert, S., & Ruiz, M. T. 1992, *RevMexAA*, 24, 155
- Péquignot, D., Petitjean, P., & Boisson, C. 1991, *A&A*, 251, 680
- Quinet, P. 1996, *A&AS*, 116, 573
- Reifenstein, E. C., Wilson, T. L., Burke, B. F., Mezger, P. G., & Altenhoff, W. J. 1970, *A&A*, 4, 357
- Robertson-Tessi, M., & Garnett, D. R. 2005, *ApJS*, 157, 371
- Rodríguez, M. 1996, *A&A*, 313, L5
- _____. 1999a, *A&A*, 348, 222
- _____. 1999b, *A&A*, 351, 1075
- _____. 2002, *A&A*, 389, 556
- Rubin, R. H. 1969, *ApJ*, 155, 841
- Ruiz, M. T., Peimbert, A., Peimbert, M., & Esteban, C. 2003, *ApJ*, 595, 247
- Sánchez, L. J., & Peimbert, M. 1991, *RevMexAA*, 22, 285
- Sawey, P. M. J., & Berrington, K. A. 1993, *At. Data Nucl. Data Tables*, 55, 81
- Seaton, M. J. 1979, *MNRAS*, 187, 73P
- Shaver, P. A., & Goss, W. M. 1970, *Aust. J. Phys. Astrophys. Supp.*, 14, 133
- Shaw, R. A., & Dufour, R. J. 1995, *PASP*, 107, 896
- Smits, D. P. 1996, *MNRAS*, 278, 683
- Storey, P. J. 1994, *A&A*, 282, 999
- Storey, P. J., & Hummer, D. G. 1995, *MNRAS*, 272, 41
- Torres-Peimbert, S., & Peimbert, M. 2003, in *IAU Symp. 209, Planetary Nebulae: their Evolution and Role in the Universe*, ed. S. Kwok, M. Dopita, & R. Sutherland (San Francisco: ASP), 363
- Torres-Peimbert, S., Peimbert, M., & Daltabuit, E. 1980, *ApJ*, 238, 133
- Tsamis, Y. G., Barlow, M. J., Liu, X.-W., Danziger, I. J., & Storey, P. J. 2003, *MNRAS*, 338, 687
- Tsamis, Y. G., Barlow, M. J., Liu, X.-W., Storey, P. J., & Danziger, I. J. 2004, *MNRAS*, 353, 953
- Tsamis, Y. G., & Péquignot, D. 2005, *MNRAS*, 364, 687
- Verner, E. M., Verner, D. A., Baldwin, J. A., Ferland, G. J., & Martin, P. G. 2000, *ApJ*, 543, 831
- Viegas, S. M., & Clegg, R. E. S. 1994, *MNRAS*, 271, 993
- Zhang, H. 1996, *A&AS*, 119, 523
- Zhang, Y., Liu, X.-W., Wesson, R., Storey, P. J., Liu, Y., & Danziger, I. J. 2004, *MNRAS*, 351, 935

César Esteban and Jorge García-Rojas: Instituto de Astrofísica de Canarias, Vía Láctea s/n, E-38200, La Laguna, Tenerife, Spain (cel, jogarcia@iac.es).

Antonio Peimbert and Manuel Peimbert: Instituto de Astronomía, Universidad Nacional Autónoma de México, Apdo. Postal 70-264, 04510 México, D. F., Mexico (antonio, peimbert@astroscu.unam.mx).

Mónica Rodríguez: Instituto Nacional de Astrofísica, Óptica y Electrónica, Apdo. Postal 51 y 216, 72000 Puebla, Mexico (mrodri@inaoep.mx).

María Teresa Ruiz: Departamento de Astronomía, Universidad de Chile, Casilla Postal 36D, Santiago de Chile, Chile (mtruiz@das.uchile.cl).